Global Distributions and Changes in Stratospheric Particles

Sophie Godin, Lamont Poole, Slimane Bekki, Terry Deshler, Niels Larsen, Thomas Peter

CHAPTER 3

Global Distributions and Changes in Stratospheric Particles

Lead Authors:
S. Godin
L.R. Poole

Coauthors:
S. Bekki
T. Deshler
N. Larsen
T. Peter

Contributors:
A. Adriani
J. Barnes
R. Bevilacqua
C. David
G. Di Donfrancesco
M. Fromm
M. Hervig
H. Jäger
B. Luo
R. Neuber
M. Osborn
W. Renger
L. Thomason
O. Uchino
M. Wirth

CHAPTER 3

GLOBAL DISTRIBUTIONS AND CHANGES IN STRATOSPHERIC PARTICLES

Contents

SCIENTIFIC SUMMARY

Much progress has been made recently in our understanding of the two major classes of stratospheric particles: stratospheric sulfate aerosol (SSA), and polar stratospheric clouds (PSCs). Thermodynamic models have provided a clearer picture of particle behavior at low temperatures, while a richer and longer measurement suite has increased our knowledge of particle formation processes, the dispersal and decay of volcanic SSA, and particle climatology.

- There is no clear trend in background SSA from 1979 to 1997. SSA levels in late 1997 were below those observed before the 1991 Mt. Pinatubo eruption and are likely still decreasing. Hence, any anthropogenic contribution to the SSA layer must be smaller than previously estimated from observed changes from 1979 to 1989. Peak aerosol scattering ratios in 1997 were about 40% greater than those observed during 1979, but due to uncertainties and natural variability in the measurements, this difference must be viewed with caution at present.

- It is not clear that the 1979 minimum SSA period was truly free of volcanic influence. Recent model calculations of SSA production from known tropospheric sulfur sources significantly underestimate the 1979 observations. Other non-volcanic sources are thought to be insignificant.

- Post-volcanic SSA decay varies with time, space, and aerosol property. The e^{-1} decay time for column backscatter following the eruption of Mt. Pinatubo was about 1 year until 1994, and nearly twice as long (1.8 years) from 1994 to 1997. Derived surface areas decayed back to pre-Pinatubo levels in about 3.5 years at 25 km and about 5 years at 15 km. Surface area decayed 20-30% more slowly than backscatter or mass.

- PSC observations are still divided into two broad classes: Type 1 PSCs, containing nitric acid (HNO_3) as a major component, that form at temperatures above the water (H_2O) ice point; and Type 2 PSCs, containing predominantly H_2O ice particles. Most of the observations of Type 1 PSCs can be subclassified as Type 1b liquid particles or Type 1a solid particles. Other types of particles have been proposed to explain some specific observations.

- It is now generally accepted that Type 1b PSCs are supercooled ternary solution (STS) droplets that form from SSA without a nucleation barrier. Type 1a PSC particles are generally interpreted as solid nitric acid trihydrate (NAT), but understanding of the phase transition mechanisms leading to their formation is still poor. Better understanding of Type 1a PSCs is needed because solid particles play a significant role in denitrification.

- Many of the Type 1b PSC observations occurred during ongoing fast synoptic cooling events, shortly after the air parcels experienced cold temperatures. Type 1a PSCs, in contrast, have been observed when synoptic temperatures were below the NAT existence temperature for several days. It now appears that theoretical models of Type 1a PSC formation may require knowledge of the air parcel thermal history.

- Mesoscale temperature fluctuations, especially over mountain ranges where such fluctuations can reach 20 K peak-to-peak, are important in PSC formation processes, particularly in the Arctic. The integral effect of such phenomena on polar ozone depletion is still unclear.

- Increases in source gases and cooling of the lower stratosphere from ozone depletion and increasing greenhouse gases favor increased formation and persistence of PSCs. However, an upward trend in PSC occurrence is not discernible in the present satellite data record due to the relatively short length of the record as well as the large variability in cloud sightings from year to year.

3.1 INTRODUCTION

Since the discovery of the Antarctic ozone hole, a collection of field observations, laboratory measurements, and modeling studies has provided compelling evidence that suspended particles play a key role in halogen activation and nitrogen deactivation and, hence, ozone depletion in the lower stratosphere. Two major classes of particles are observed in this altitude region: the stratospheric sulfate aerosol (SSA), which are present at all latitudes and are enhanced periodically by volcanic eruptions, and polar stratospheric clouds (PSCs), which form during both polar winters and on into the austral polar spring. Other less abundant stratospheric particle types include cirrus clouds, soot, and rocket exhaust particles.

The effect of these particles on ozone chemistry is highly dependent on their concentration, size, phase, and composition. Hence, an understanding of ozone trends requires an understanding of these characteristics. Many measurements have been obtained in recent years that have increased our knowledge of stratospheric particles. In parallel, various techniques have been developed to derive from these measurements the particle properties needed to represent heterogeneous processes in assessment models, primarily surface area and volume. Furthermore, the 1991 eruption of Mt. Pinatubo, one of the strongest volcanic eruptions of this century, provided the opportunity to better assess the nature of volcanic SSA, its dispersal and decay, and its effects on ozone under conditions of increasing anthropogenic chlorine. This chapter reviews our knowledge of stratospheric particles and assesses our ability to evaluate and predict their formation and evolution. It deals with basic thermodynamics of the major classes of particles, their sources and possible trends, and describes in situ and remotely sensed particle observations. Outstanding issues in stratospheric particles are highlighted as well. Chapter 7 provides more discussion on particle microphysics and treats the role of particles in ozone depletion, including chlorine activation, denitrification, and dehydration. The possible influence of aircraft emissions on stratospheric particles will be dealt with in a forthcoming Intergovernmental Panel on Climate Change special report (IPCC, 1999) and, hence, will not be discussed in detail herein.

3.1.1 Types of Stratospheric Particles

The most prevalent stratospheric particles are the sub-micron-sized liquid SSA droplets composed of sulfuric acid (H_2SO_4) and H_2O. They are present continuously at all latitudes between the tropopause and about 30 km. During volcanically quiescent periods, the vertical distribution of SSA relative to tropopause height is very similar at all latitudes, with a typical radius (r) of 0.1 μm, mass mixing ratio of 10^{-9}, and number density of 10 cm^{-3} (Turco *et al.*, 1982; Hofmann, 1990a).

The other major class of stratospheric particles is PSCs, which are observed in cold regions of the lower polar stratosphere, primarily during winter. On the basis of their optical properties, PSCs have been further divided into two distinct subclasses: Type 1 PSCs that are thought to be relatively small particles containing nitric acid (HNO_3) as a major component, and Type 2 PSCs that are larger, primarily H_2O ice particles. Typical mass mixing ratios for Type 1 and Type 2 PSCs are 10^{-8} and 10^{-6}, respectively (Turco *et al.*, 1989).

Cirrus clouds also occur near the tropopause and perhaps in the lowest part of the stratosphere in middle and high latitudes, as shown by an analysis of extinction data from the Stratospheric Aerosol and Gas Experiment (SAGE) II (Wang *et al.*, 1996). Studies by Borrmann *et al.* (1996, 1997a) suggest that heterogeneous reactions on the surfaces of these clouds can cause changes in chemical composition akin to those induced by Type 2 PSCs in the polar stratosphere. A follow-on study by Solomon *et al.* (1997) suggests that cirrus can also lead to ozone depletion near the tropopause if they occur with sufficient frequency and spatial extent. The largest effect of cirrus on ozone would be expected near the midlatitude tropopause of the Northern Hemisphere in summer.

Recently, some attention has also been focused on soot, because these particles could act as cloud condensation nuclei and also provide reactive surfaces for heterogeneous chemistry (Bekki, 1995; Blake and Kato, 1995; Pueschel, 1996). Maximum soot concentrations greater than 1 ng m^{-3} are found at northern midlatitudes at altitudes of about 10 km. Some of the soot particles are expected to end up embedded in H_2SO_4/H_2O solution via coagulation with H_2SO_4/H_2O aerosols and, possibly, condensation of gaseous H_2SO_4.

Model calculations indicate that the impact on the stratospheric aerosol layer of solid particles emitted by rocket and Space Shuttle launches is likely to be very modest (Jones *et al.*, 1995; Jackman *et al.*, 1996).

3.1.2 SSA and PSC Thermodynamics

3.1.2.1 SSA

Production of SSA droplets begins primarily with the oxidation of gaseous sulfur-bearing compounds such as carbonyl sulfide (OCS) or sulfur dioxide (SO_2). The end oxidation product, gaseous H_2SO_4, has a very low saturation vapor pressure and therefore takes a particulate form in the lower stratosphere. The exact mechanism of gas-to-particle conversion has not been fully elucidated. New SSA could be formed in situ either by homogeneous nucleation or heterogeneous nucleation on solid materials present in the stratosphere, such as volcanic ash, micrometeorites, aluminum oxide, or soot (Turco *et al.*, 1982; Zolensky *et al.*, 1989; Blake and Kato, 1995; Pueschel, 1996). Traces of foreign materials that have been detected in some SSA (Turco *et al.*, 1982) are not necessarily indicative of heterogeneous nucleation, however, because foreign materials can also be introduced through coagulation.

There is some observational evidence for in situ homogeneous nucleation. For example, after the eruption of Mt. Pinatubo in 1991, increases by up to 2 orders of magnitude in the concentration of condensation nuclei (CN) were observed in the volcanic layers, with 95-98% of the particles composed of H_2SO_4 and H_2O according to volatility experiments (Deshler *et al.*, 1992). Electron microscope analysis of these particles revealed that most of the fine particles did not show any evidence of solid or dissolved nucleus material (Sheridan *et al.*, 1992), suggesting that homogeneous nucleation was the main aerosol production mechanism in the Mt. Pinatubo plume. Unusually large increases in CN concentration, likely indicative of nucleation events, have also been detected at about 25-30 km during winter and early spring in northern middle and polar latitudes (Hofmann and Rosen, 1982; Hofmann *et al.*, 1985; Hofmann, 1990b), as well as during spring over Antarctica (Hofmann *et al.*, 1988; Wilson *et al.*, 1989; Deshler *et al.*, 1994a). Such increases in CN concentration seemed to be more intense during volcanic periods. Model calculations suggest that these enhanced CN layers are produced by binary homogeneous nucleation triggered by either subsidence of sulfur-rich air in the cold polar vortex (Zhao *et al.*, 1995) or by a rapid cooling following a polar stratospheric warming (Hofmann and Rosen, 1983; Bekki *et al.*, 1997).

Overall, conditions favorable for homogeneous SSA nucleation, such as highly enhanced gaseous H_2SO_4 levels, rapid temperature fluctuations around the evaporation/condensation point, and very low pre-existing particle surface area density, occur infrequently in the stratosphere except in the early stages of a volcanic plume or at the top of the SSA layer. Atmospheric observations and calculations suggest that the upper tropical troposphere is a major source of CN and as such governs the number concentration of SSA in the lower tropical and midlatitude stratosphere (Brock *et al.*, 1995).

Once formed, SSA droplets grow by coagulation and co-condensation of H_2SO_4 and H_2O. They are removed from the stratosphere through a combination of gravitational sedimentation and stratospheric-tropospheric exchange. As shown by modeling studies (e.g., Turco *et al.*, 1979; Bekki and Pyle, 1992; Pitari *et al.*, 1993; Tie *et al.*, 1994; Weisenstein *et al.*, 1997), the interplay between growth by condensation, coagulation, and removal of the large aerosol particles by sedimentation leads to the establishment of the well-known unimodal lognormal particle size distribution with a typical mode radius of about 0.08 μm and a typical geometric standard deviation of about 1.8. At typical stratospheric conditions (200 K < T < 240 K), liquid SSA have theoretical compositions ranging from 60 to 80% H_2SO_4 by weight. Because H_2O is present in much higher concentrations in the atmosphere than H_2SO_4, SSA composition can be assumed to be determined by temperature and humidity only (Steele and Hamill, 1981; Carslaw *et al.*, 1997).

Frozen H_2SO_4 hydrates are the thermodynamically stable phases in the stratosphere (Gable *et al.*, 1950; Zhang *et al.*, 1993). Sulfuric acid tetrahydrate (SAT = $H_2SO_4 \cdot 4H_2O$) is the favored hydrate under polar winter conditions but is expected to melt at about 220 K upon heating (Middlebrook *et al.*, 1993; Zhang *et al.*, 1993). However, most observations suggest that SSA are, indeed, supercooled liquid droplets rather than solid crystals. This is consistent with laboratory experiments showing that, despite the thermodynamic stability of H_2SO_4 hydrates, liquid H_2SO_4/H_2O solutions do not freeze readily, even when highly supercooled (Molina *et al.*, 1993; Anthony *et al.*, 1995; Koop *et al.*, 1997) or when certain solid nuclei are present (Koop *et al.*, 1995; Biermann *et al.*, 1996). Theoretical studies reach a simi-

lar conclusion, i.e., that homogeneous freezing of a pure H_2SO_4/H_2O solution to form SAT is hindered energetically (Luo *et al.*, 1994; MacKenzie *et al.*, 1995). Freezing of H_2SO_4/H_2O solutions might be somewhat facilitated by HNO_3 uptake at low temperatures close to the frost point, T_{ice} (Molina *et al.*, 1993; Beyer *et al.*, 1994; Iraci *et al.*, 1995), although other studies suggest that this might not be sufficient for droplets to freeze (Koop *et al.*, 1995). A temperature hysteresis in the life-cycle of SSA particles with freezing close to T_{ice} and melting at about 215-220 K has been indicated from balloonborne backscatter measurements (Larsen *et al.*, 1995).

3.1.2.2 TYPE 1 PSCS

According to the phase diagram of Hanson and Mauersberger (1988) and in the absence of phase transition barriers, gaseous HNO_3 and H_2O would be expected to co-condense to form a stable solid phase, nitric acid trihydrate (NAT = $HNO_3 \cdot 3H_2O$) at about 195 K in the polar stratosphere. Because homogeneous nucleation of HNO_3 and H_2O vapors is not favored energetically, pre-existing solid particles, possibly SAT, were previously believed to act as condensation nuclei for NAT. However, laboratory and theoretical studies later indicated that heterogeneous nucleation of NAT on SAT is rather unlikely even at high NAT supersaturations (Iraci *et al.*, 1995; MacKenzie *et al.*, 1995). Some pre-activation of SAT by a previous exposure to NAT may, however, reduce the level of supersaturation required for NAT condensation (Zhang *et al.*, 1996). These results combined with the fact that liquid H_2SO_4/H_2O solutions do not freeze readily suggest that particles may remain liquid well below the NAT existence temperature (T_{NAT}) and solid particles, composed of acid hydrates and ice, only form at lower temperatures close to or below T_{ice}.

Thermodynamic models using laboratory data predict a steep increase in HNO_3 solubility into liquid H_2SO_4/H_2O solutions a few degrees below T_{NAT} (Beyer *et al.*, 1994; Carslaw *et al.*, 1994; Tabazadeh *et al.*, 1994; Luo *et al.*, 1995), leading to the formation of supercooled ternary ($HNO_3/H_2SO_4/H_2O$) solution (STS) droplets. This mechanism is illustrated in Figure 3-1, where the equilibrium state of a droplet ensemble is shown between 260 K and 185 K at the 55-hPa pressure level. Above approximately 260 K, the liquid fully evaporates, which explains the evaporation of droplets at the upper boundary of the Junge particle layer, while at 3-4 K below the frost point, H_2O ice and possibly acid hydrates precipitate. From 250 K to below 188 K, liquid droplets can exist in the stratosphere and undergo some remarkable changes. Below 250 K virtually all the H_2SO_4 condenses, leading to small, highly concentrated H_2SO_4/H_2O droplets that dilute as the temperature decreases (Steele and Hamill, 1981). At 196 K, T_{NAT} is reached (arrow in Figure 3-1a), and NAT would be expected to grow readily

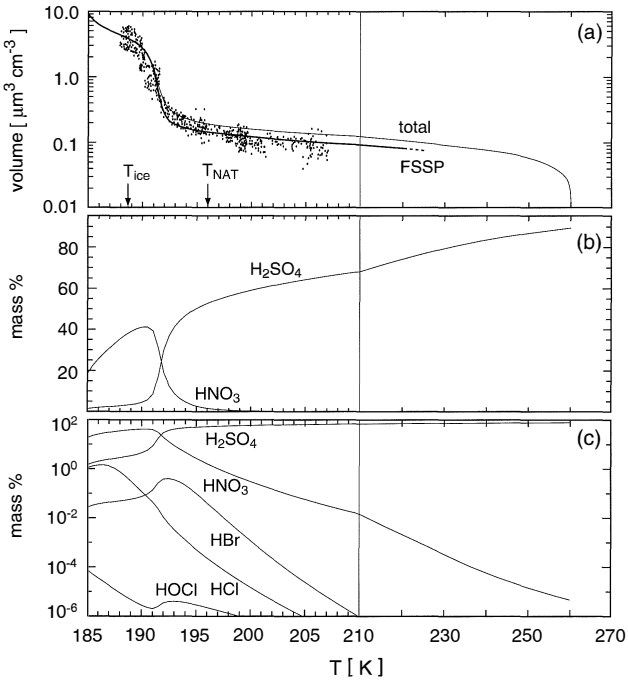

Figure 3-1. Partitioning of stratospheric gases into liquid stratospheric aerosols: (a) total aerosol volume; (b) H_2SO_4 and HNO_3 liquid concentrations in weight percentage; (c) same as (b) but on logarithmic scale and including hydrochloric acid (HCl), hypochlorous acid (HOCl), and hydrogen bromide (HBr) concentrations. Results for $T < 210$ K are from Carslaw *et al.* (1997), and those for H_2SO_4 at $T > 210$ K are from Ayers *et al.* (1980). Atmospheric conditions are 55 hPa pressure, 5 ppm H_2O, 10 ppb HNO_3, 0.5 ppb H_2SO_4, 1 ppb HCl, 10 ppt HOCl, and 10 ppt HBr. The frost point (T_{ice}) and NAT existence temperature (T_{NAT}) are indicated by vertical arrows. In addition to total volume, panel (a) shows ER-2 measurements of 24 January 1989 (Dye *et al.*, 1992) and the modeled aerosol volume in the observation window of the forward scattering spectrometer probe (FSSP) instrument (0.2 µm < r < 10 µm).

in the absence of a nucleation barrier, accompanied by a sharp increase in particle volume and an almost complete removal of HNO_3 from the gas phase. In contrast, the liquid phase, even at 193 K is still mainly H_2SO_4/H_2O. However, at lower temperatures between 193 K and 190 K, increasing solubilities enable a strong, coupled uptake of gas-phase HNO_3 and H_2O. This uptake transforms the solution within this interval from quasi-binary H_2SO_4/H_2O into quasi-binary HNO_3/H_2O with about 40% HNO_3 by weight and less than 3% H_2SO_4 by weight. The liquid volume grows by a factor of 10, as was observed during the flight of the National Aeronautics and Space Administration (NASA) Earth Resources-2 (ER-2) aircraft on 24 January 1989 (Dye *et al.*, 1992) (data points in Figure 3-1a). As the temperature drops further toward T_{ice}, the remaining HNO_3 is readily taken up, and the droplets grow to a total volume higher than that of NAT in equilibrium. Figure 3-1c also shows the uptake of other species that are of primary importance for heterogeneous chemistry. Type 1b clouds are highly efficient processors of halogen species (see Chapter 7). Because some field observations of Type 1 PSCs cannot be explained in terms of NAT or STS clouds in equilibrium, other metastable phases in equilibrium (Tabazadeh *et al.*, 1995) or highly nonequilibrium particles (Meilinger *et al.*, 1995; Peter, 1997) have been proposed as explanations. STS droplets or other metastable particles would not coexist for long with NAT particles because NAT particles would be expected to grow slowly at the expense of the other particles due to lower NAT saturation vapor pressures.

3.1.2.3 Type 2 PSCs

It is now fairly well established that Type 2 PSCs are primarily water ice particles. Laboratory experiments (Koop *et al.*, 1995) suggest that ice nucleates inside liquid Type 1 PSC particles or on the surface of solid Type 1 PSC particles once the temperature falls to 2-4 K below T_{ice}. The reason for this rather well-constrained relationship between temperature and ice nucleation is the onset of strong uptake of H_2O by binary or ternary solutions at these temperatures, leading to highly diluted, water-like droplets that must freeze. A supercooling of about 4 K below T_{ice} has recently also been observed (Carslaw *et al.*, 1998) during the formation of mountain-wave-induced Type 2 clouds (see Sections 3.4.3 and 7.4.1).

Once formed, ice particles develop further according to well-known thermodynamics. However, despite the close coupling between temperature and ice formation, the remaining uncertainty in supercooling is still a critical issue. Whether ice formation begins at 2 K or at 4 K of supercooling determines the extent of ice cloud occurrence, particularly in the Arctic, and is also likely to influence the particle number density in individual clouds and, thus, their optical and chemical properties. This is similar to open issues in our understanding of cirrus cloud formation in the upper troposphere.

After ice nucleation from liquid ternary solution droplets, the fate of the acidic components (HNO_3, H_2SO_4) is not well known. In some particles they might freeze as NAT and SAT (Koop *et al.*, 1995, 1997), while in others some of the HNO_3 might partition back into the gas phase and the remaining acid might stay as a liquid coating on the ice particle (Carslaw *et al.*, 1998). Furthermore, it is not clear whether soluble species such as HNO_3 could be trapped within the ice matrix or to what extent such species might lead to a solid coating of ice particles, influencing their microphysical properties (see Chapter 7).

3.1.3 Particle Source Gases

3.1.3.1 Sulfur

The predominant source of SSA in the stratosphere is strong, sulfur-rich volcanic eruptions, which are by nature highly intermittent and unpredictable. The average flux of volcanic sulfur (S) to the stratosphere over the last 200 years has been estimated to be around 1 Tg yr^{-1} S, with lower and upper bounds of 0.3 and 3 Tg yr^{-1} (Pyle *et al.*, 1996). A minimum flux of 0.5-1 Tg yr^{-1} S for the past 9000 years has been derived from ice core sulfate data. There have been two large sulfur-rich eruptions in the last two decades: El Chichón in 1982 (3.5 Tg S) and Mt. Pinatubo in 1991 (9 Tg S).

OCS oxidation is believed to be the major non-volcanic source of stratospheric sulfur (Crutzen, 1976). Recent estimates of this source range from 0.03 Tg yr^{-1} S (Chin and Davis, 1995) to 0.049 Tg yr^{-1} S (Weisenstein *et al.*, 1997). Although most OCS sources are natural, there are some indications that anthropogenic emissions of OCS may be substantial, and possibly increasing (Khalil and Rasmussen, 1984; Zander *et al.*, 1988; Hofmann, 1990a). However, historical data on industrial releases suggest that anthropogenic emissions of OCS and its precursor carbon disulfide (CS_2) have been relatively constant over the 1977-1992 period (Chin and Davis, 1993). Furthermore, no statistically significant

trend in lower stratospheric OCS was inferred from spaceborne observations made in 1985 and 1994 (Rinsland *et al.*, 1996).

Other surface sources of sulfur are approximately 3 orders of magnitude larger than the OCS source. Although most reduced sulfur gases other than OCS are rapidly oxidized to SO_2 and therefore are not expected to reach the stratosphere in large amounts, 2-D model calculations suggest that the stratospheric aerosol loading may be strongly influenced by upper tropospheric sulfur (Weisenstein *et al.*, 1997). However, large uncertainties are associated with tropospheric sulfur chemistry, tropospheric removal, vertical transport of short-lived species (Langner and Rodhe, 1991), and stratospheric-tropospheric exchange (Holton *et al.*, 1995). Such uncertainties reduce the level of confidence in model assessments of the impact of the massive surface emissions of short-lived sulfur (CS_2, dimethyl sulfide (DMS), hydrogen sulfide (H_2S), SO_2) on the stratosphere.

3.1.3.2 Nitric Acid

Nitrous oxide (N_2O) is the principal precursor of stratospheric reactive nitrogen (NO_y) and hence of HNO_3. Anthropogenic emissions of N_2O stem primarily from agricultural sources and are about half as large as natural emissions. The rate of NO_y production from N_2O oxidation is approximately 0.5-1 Tg yr^{-1} N (Kasibhatla *et al.*, 1991; WMO, 1995; Vitt and Jackman, 1996). N_2O concentrations are increasing at a rate of about 0.25% yr^{-1} (WMO, 1995; IPCC, 1996). Lightning may also be another significant, though uncertain, source of nitrogen in the tropical lower stratosphere (Kotamarthi *et al.*, 1994).

3.1.3.3 Water Vapor

The main sources of H_2O to the stratosphere are thought to be injection through the tropical tropopause and in situ production from methane (CH_4) oxidation (Harries *et al.*, 1996). Stratospheric-tropospheric exchange at middle and high latitudes might also be important. Direct evidence of the link between the tropical H_2O distribution and the annual cycle in tropopause temperature has been provided by satellite data (Mote *et al.*, 1995, 1996). The average H_2O mixing ratio of air entering the stratosphere inferred from satellite, aircraft, and balloon data ranges from 3.2 to 4.2 parts per million (ppm) (Dessler *et al.*, 1994; Abbas *et al.*, 1996; Engel *et al.*, 1996; Mote *et al.*, 1996; Remsberg *et al.*, 1996). Because, to first order, two molecules of H_2O can be formed from one of CH_4, the quantity $H_2O + 2CH_4$ is approximately conserved over the lower and middle stratosphere at a value of 6.7 to 7.6 ppm, as shown by satellite and aircraft observations. Tropospheric CH_4 has been increasing at an average rate of 0.6% yr^{-1} over the last 10 years (IPCC, 1996). Because production of H_2O by CH_4 oxidation is relatively small in the lower stratosphere, any H_2O trend there should be substantially smaller than the CH_4 trend.

A statistically significant upward trend in H_2O concentration has been detected at altitudes from 16 to 26 km at northern midlatitudes from balloonborne hygrometer measurements carried out from 1981 to 1994 (Oltmans and Hofmann, 1995). The maximum trend was found to be 0.8% yr^{-1} at 18-20 km. This finding is corroborated by an apparent increase in $H_2O + 2\ CH_4$ derived from a variety of measurements made since 1975 (Engel *et al.*, 1996). However, the H_2O trend seems to be larger than the trend expected from the oxidation of increased CH_4 alone (Oltmans and Hofmann, 1995; Engel *et al.*, 1996). Nedoluha *et al.* (1998) also reported an upward trend in H_2O in the stratosphere based on Halogen Occultation Experiment (HALOE) and ground-based millimeter-wave spectrometer data.

3.2 INSTRUMENTS

3.2.1 Measurement Principles

Instruments to measure SSA can be broadly divided into two categories, those that provide ensemble measurements and those that provide individual particle measurements. Ensemble measurements detect the signature of a population of particles at one instant and include passive extinction measurements, such as from the sunphotometer (Volz and Goody, 1962), and active scattering measurements, such as lidar (Fiocco and Grams, 1964). Individual measurements include those that use optical scattering to count and size single particles (Rosen, 1964; Baumgardner *et al.*, 1992) and those that use impaction to collect particles that can then be counted, sized, and chemically analyzed (Bigg, 1975; Farlow *et al.*, 1979). The range of instruments available allows for a variety of measurement platforms. Ensemble measurements are usually conducted on the ground for high temporal and vertical resolution, or from satellites for global coverage. Single-particle measurements are usually conducted using aircraft for high vertical and

horizontal resolution, or balloons for high vertical resolution and accessibility to regions of the stratosphere above aircraft altitudes.

3.2.2 Contemporary Data Records

Regular measurements using ground-based lidar began in the early 1970s, and some of these records extend to the present (Jäger, 1991; Osborn *et al.*, 1995; Barnes and Hofmann, 1997). Lidars provide high-vertical-resolution measurements of particle backscatter, and often depolarization ratio as well, at one or more wavelengths. Lidar sites now range in latitude from 90°S to 79°N, with a number of sites in the low to midlatitudes, and a few stations in the subtropics. Sunphotometer measurements began in the 1950s and extend to the present. Aerosol optical depth is usually measured at several wavelengths and can then be used to infer column size distributions. Long-term ground-based measurements are available from polar (Herber *et al.*, 1993) and tropical regions (Russell *et al.*, 1993a), and sunphotometers have been deployed on aircraft as well (Russell *et al.*, 1993b).

Aerosol extinction measurements from spaceborne platforms began in 1975 (Pepin *et al.*, 1977). These became routine with the launch of the autonomous limb-viewing optical extinction instruments, Stratospheric Aerosol Measurement (SAM) II and SAGE, in 1979 (McCormick *et al.*, 1979). The near-global, multi-wavelength measurements from SAGE and its successor SAGE II cover the periods 1979-1981 and 1984 to the present, respectively. The single-wavelength record from SAM II, whose spatial coverage was limited to high latitudes, extends continuously from 1978 to 1991, with intermittent data thereafter until late 1993. Satellite extinction measurements were expanded in 1991 with the launch of the Upper Atmosphere Research Satellite (UARS), carrying HALOE, which measures infrared limb extinction, and CLAES (Cryogenic Limb Array Etalon Spectrometer) and ISAMS (Improved Stratospheric and Mesospheric Sounder), which measure infrared limb emission (see *Geophysical Research Letters*, *Vol. 20*, No. 12, 1993). The lifetimes of CLAES and ISAMS were limited to less than two years, but HALOE is still operational. High-resolution middle-infrared measurements of extinction by Mt. Pinatubo SSA were made by the Atmospheric Trace Molecule Spectroscopy (ATMOS) instrument during a March-April 1992 Space Shuttle mission (Rinsland *et al.*, 1994). High-latitude solar occultation aerosol measurements were also made from 1993-1996 by the Polar Ozone and Aerosol Measurement (POAM) II instrument on the French SPOT (Satellite Pour l'Observation de la Terre) 3 satellite (Glaccum *et al.*, 1996). More recently there are new infrared extinction measurements available from ILAS (Improved Limb Atmospheric Spectrometer) on the Japanese ADEOS (Advanced Earth Observing Satellite) platform from August 1996 to June 1997. The nadir-viewing AVHRR (Advanced Very High Resolution Radiometer) satellite instruments measure the reflected solar radiance and infer aerosol optical thickness (Griggs, 1983). These observations have a fine horizontal resolution over oceans for tracking dense volcanic clouds but cannot provide any vertical resolution (Stowe *et al.*, 1992).

Individual particle measurements are obtained in situ with aerosol spectrometers. Spectrometers deployed on aircraft include ones with sampling volumes external to the instrument ($0.15\ \mu m < r < 10\ \mu m$) (Baumgardner *et al.*, 1992) and those with internal sampling volumes ($0.03\ \mu m < r < 1.0\ \mu m$) (Jonsson *et al.*, 1995). Particle counters carried on balloons require internal sampling volumes ($0.15\ \mu m < r < 10\ \mu m$) (Hofmann *et al.*, 1975; Hofmann and Deshler, 1991). In situ sampling is also done using impaction devices on aircraft (Pueschel *et al.*, 1989; Sheridan *et al.*, 1994) and on balloons (Sheridan *et al.*, 1992). The physical samples collected by the impaction devices are returned to the laboratory for analysis. Regular stratospheric aerosol measurements using aerosol counters carried on balloon platforms have continued since the 1970s (Hofmann, 1990a; Deshler *et al.*, 1997). Aerosol impactors carried on balloons are employed much less frequently (Bigg, 1975; Sheridan *et al.*, 1992). Stratospheric aerosol measurements using aircraft-borne aerosol spectrometers began with the investigations of polar ozone loss in 1987 and 1989 (Dye *et al.*, 1990a; Wilson *et al.*, 1992) and have continued through the eruption of Mt. Pinatubo (Jonsson *et al.*, 1996). Aerosol impactors on aircraft have been used since the late 1970s (Farlow *et al.*, 1979; Goodman *et al.*, 1994). In number concentration, a large fraction of aerosol has sizes below the minimum sizes detectable with optical instruments. To measure the concentration of these CN, diffusion chambers are placed ahead of optical counters to grow all available particles to optically detectable sizes prior to counting (Rosen and Hofmann, 1977; Wilson *et al.*, 1983). Although CN counters do not discriminate particles according to size,

laboratory tests indicate they are sensitive to particles with $r > 0.01$ μm at stratospheric pressures (Wilson *et al.*, 1983). The first regular sampling of stratospheric CN began in the mid-1970s from balloons and in the 1980s from aircraft. A balloonborne backscattersonde combines in situ methods with an ensemble measurement (Rosen and Kjome, 1991). These instruments have been used in the 1990s for regular midlatitude measurements (Rosen *et al.*, 1994a) and for seasonal Arctic measurements (Larsen *et al.*, 1997).

3.2.3 Derivation of Particle Characteristics

For many applications the directly measured particle properties, i.e., extinction, scattering, number, or size, are not the quantities required. In particular, heterogeneous chemical reaction rates may be a function of aerosol surface area or volume, depending on the ratio of the molecular diffusion coefficient to the molecular loss rate coefficient (Hanson *et al.*, 1994). For example, the reaction of chlorine nitrate ($ClONO_2$) with hydrochloric acid (HCl) dissolved in SSA seems to depend on aerosol volume, whereas the hydrolysis of dinitrogen pentoxide (N_2O_5) on SSA is fast enough that only aerosol surface area is important. At cold temperatures, particle phase is also important, because the effective uptake coefficient is smaller on solid hydrates than on liquid particles at the same temperature (Ravishankara and Hanson, 1996; Borrmann *et al.*, 1997b). Phase is also important when considering particle growth rates, because STS droplets can be quite a bit smaller than solid HNO_3 hydrate particles.

3.2.3.1 Surface Area and Volume

Aerosol surface area and volume concentrations can be obtained from individual particle measurements either by directly integrating the measured discrete size distribution (Dye *et al.*, 1992; Pueschel *et al.*, 1992; Wilson *et al.*, 1993; Goodman *et al.*, 1994; Jonsson *et al.*, 1995) or by fitting measured particle number concentrations with an analytic size distribution function and integrating (Deshler *et al.*, 1993). The uncertainties of 30-50% estimated for surface area and volume obtained in this way arise from Poisson counting statistics at low concentrations, and from sizing errors. The sizing errors (10-20%) arise primarily from uncertainties in particle refractive index, from inhomogeneities in particle illumination, and from spectral broadening (Baumgardner *et al.*, 1992). Discrete size distributions measured simultaneously by several individual particle measurement techniques have been compared and found to agree favorably when differences in sampling technique are accounted for (Pueschel *et al.*, 1992).

Because the wavelength dependence of extinction is related to particle size (Ångström, 1908), in situ individual and remote ensemble particle measurements can be compared using Mie scattering theory. One approach is to compare satellite extinction measurements to extinctions calculated using discrete and fitted size distributions derived from particle counter data (Wilson *et al.*, 1992; Jonsson *et al.*, 1995; Hervig *et al.*, 1996). The opposite approach is to derive particle size information by inverting multi-wavelength extinction, scattering, or emission data. Twomey (1974) and Capps *et al.* (1982) concluded that extinction measurements at a few wavelengths cannot be expected to yield detailed information about the particle size distribution, but can be used to reliably estimate moments of the distribution. The inversion of multi-wavelength extinction/scattering measurements is complex, and a number of techniques have been tried (Grainger *et al.*, 1995; Yue *et al.*, 1995; Anderson and Saxena, 1996). For estimating surface area or volume using four-wavelength SAGE II extinction data, Thomason and Poole (1993) found that principal component analysis (Twomey, 1977) worked well. Uncertainties in volume and surface area estimated in this way were shown to be ~30%. Other recent estimates of surface area and volume have been made using multi-wavelength lidar data (e.g., Del Guasta *et al.*, 1994; Stein *et al.*, 1994; Gobbi, 1995; Wandinger *et al.*, 1995) and HALOE infrared extinction measurements (Hervig *et al.*, 1997). These estimates were made using empirical relationships established from Mie scattering calculations performed with a large set of observed size distributions. Uncertainties on these surface area estimates are around 30% as well.

Figure 3-2 shows comparisons of surface area and volume estimated from in situ optical particle counter data over Laramie, Wyoming (41°N), and from relevant SAGE II and HALOE satellite extinction measurements (Thomason *et al.*, 1997a; Hervig *et al.*, 1998). These comparisons show differences of roughly 50%, with the satellite estimates typically greater than the particle counter data. Another study of closure among various measurement approaches (Russell *et al.*, 1996) showed that during the 2 years following the Mt. Pinatubo eruption, the area-weighted, or effective, particle radius de-

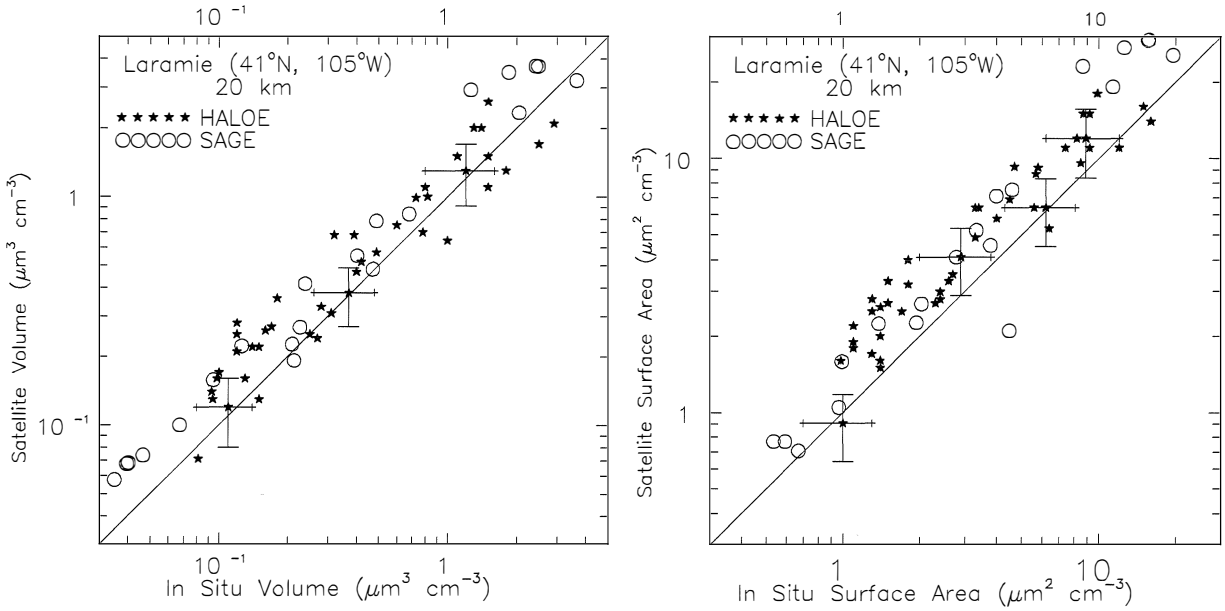

Figure 3-2. Volumes and surface areas inferred from satellite measurements of visible (SAGE II) and infrared (HALOE) extinction compared with balloonborne optical particle counter measurements over Laramie, Wyoming (41°N). The SAGE data are monthly medians over the 35°-45°N latitude band, while the HALOE data are chosen within a time and distance window as described in Hervig *et al.* (1997). A one-to-one agreement line and error bars of 30% are included for reference.

termined by sunphotometers, satellite instruments, airborne wire impactors, and balloonborne particle counters agreed to within roughly 25%.

3.2.3.2 Phase

Information on particle phase has been obtained to date primarily from active optical scattering measurements using polarized light. Lidar is the most common instrument with this capability, although some backscattersondes have this capability as well. Linearly polarized light is transmitted, and the returned signal is measured in both the parallel-polarized and cross-polarized channels. Depolarization from an ensemble of scatterers in excess of that expected from the molecular atmosphere is an indication that non-spherical particles are present. The standard value for molecular depolarization is 1.4% (Young, 1980), although some systems with narrowband interference filters use a limit of 0.5% (Shibata *et al.*, 1997). Depolarizing aerosol may consist of a mixture of solid and liquid particles, or of solid particles with a variety of forms. Because of size-dependent polarization properties for fixed particle shape (Mischenko and Sassen, 1998), it is difficult to quantify depolarization as a measure of the non-sphericity of the scattering particles, although some attempts have been made (Flesia *et al.*, 1994; Carslaw *et al.*, 1998). Browell *et al.* (1990) were the first to report that PSCs above the frost point could be separated into two classes based on depolarization. Stefanutti *et al.* (1991) and Adriani *et al.* (1995) made similar observations in the Antarctic. Observations of depolarized signals from Mt. Pinatubo volcanic aerosol were made in the Antarctic (Gobbi and Adriani, 1993), in northern midlatitudes (Vaughan *et al.*, 1994), and in the Arctic (Toon *et al.*, 1993; Godin *et al.*, 1994; Rosen *et al.*, 1994b). The measurements by Toon *et al.* were above the Mt. Pinatubo ash layer and those by Rosen *et al.* were obtained in January 1993 after most of the volcanic ash should have been removed from the stratosphere. These observations might therefore indicate the presence of solid H_2SO_4/H_2O particles (see Section 3.4 and Chapter 7).

3.2.3.3 Composition

The composition of SSA was first assessed using impactors to physically collect the aerosol, which could then be sized and chemically analyzed (Junge *et al.*, 1961;

Bigg, 1975). Other early methods used heaters positioned ahead of aerosol counters to evaporate the aerosol (Rosen, 1971). Determining the temperature at which the majority of aerosol evaporated to sizes below the counter limits allowed the H_2SO_4-H_2O composition to be estimated (Hofmann and Rosen, 1983). Both of these techniques have been used for recent measurements of Mt. Pinatubo aerosol (Sheridan *et al.*, 1992; Deshler *et al.*, 1993; Goodman *et al.*, 1994; Sheridan *et al.*, 1994) and of aerosol in the polar regions (Pueschel *et al.*, 1989; Goodman *et al.*, 1997), and to determine the volatile fraction of tropical CN (Brock *et al.*, 1995) and CN in aircraft plumes (Hofmann and Rosen, 1978; Fahey *et al.*, 1995). An alternate technique using ion mass spectrometry to analyze vaporized particles in situ and comparing the resultant H_2SO_4 concentrations with correlative in situ aerosol concentrations has been recently applied (Arnold *et al.*, 1998). Measurements at temperatures above 200 K are all consistent and indicate that SSA are predominantly droplets of highly concentrated H_2SO_4. Analyses of spaceborne infrared extinction and limb emission data on aerosols also show consistency with a concentrated H_2SO_4 composition (Rinsland *et al.*, 1994; Massie *et al.*, 1996).

As mentioned in Sections 3.1.2.2 and 3.1.2.3, there are still uncertainties with regard to the exact composition of PSCs. Recent approaches to determining the composition of these particles include the use of multi-angle aerosol scattering devices (Baumgardner *et al.*, 1996) and comparison of nearly coincident lidar and in situ measurements (Adriani *et al.*, 1995). These methods have both been shown to be consistent when applied to the well-known SSA, and some initial results are available for Antarctic PSC measurements.

3.3 SSA OBSERVATIONS

Direct measurements of SSA were first made in 1957 by Junge *et al.* (1961) using balloonborne impactors. The SSA layer is often called the Junge layer in recognition of these measurements. However, the existence of the layer was suggested some 50 years earlier from twilight observations (Gruner and Kleinert, 1927). As discussed previously, systematic measurements of SSA have been made from a variety of platforms since the early 1970s.

3.3.1 Volcanic Aerosol

All the contemporary data records clearly illustrate the strong perturbations to SSA levels caused by sulfur-rich volcanic eruptions (Hofmann, 1990a; Jäger, 1991; Chazette *et al.*, 1995; Osborn *et al.*, 1995; Uchino *et al.*, 1995; Thomason *et al.*, 1997b). Sulfur gases in the eruption plumes are oxidized to H_2SO_4, which then condenses into SSA within about 2 months of an eruption. Historical records spanning the last 100 years or more suggest that the most recent 30-year period can be characterized as a relatively active volcanic period. Primarily through the use of historical pyrheliometric data, Stothers (1996) showed that eight major eruptions occurred during the past century. Four of these occurred between 1880 and 1910 (Krakatau, an unidentified eruption, Santa Maria, and Katmai) and four occurred since 1960 (Agung, Fernandina, El Chichón, and Mt. Pinatubo). Between 1910 and 1960, the stratosphere was almost undisturbed by volcanic activity. Junge's measurements of the SSA layer came at the end of this period, but the contemporary long-term records did not begin until after the start of the current volcanically active period. In terms of impact on the stratosphere, the two largest eruptions in the last 100 years were Krakatau first, and then Mt. Pinatubo (Stothers, 1996). Analyses of ice cores from Greenland permit an even longer view (Hammer *et al.*, 1980), which indicates that global volcanism has an approximate 80-year periodicity. The mid-twentieth century lull in volcanism may be the most recent manifestation of this periodicity.

3.3.1.1 Dispersal of Volcanic Aerosol

The two most recent major eruptions have occurred in the tropics: El Chichón (17°N, April 1982) and Mt. Pinatubo (15°N, June 1991). However, since they occurred in different seasons and at different phases in the vertical structure of the quasi-biennial oscillation (QBO), the dispersal and decay of aerosol from the eruptions were different. A notable feature of low-latitude eruptions is the accumulation of aerosol in a tropical stratospheric reservoir (Trepte and Hitchman, 1992). This reservoir has an abrupt, narrow boundary on the winter hemisphere side and a broad boundary on the summer hemisphere side, as noted following the Mt. Pinatubo eruption (Grant *et al.*, 1996; Lambert *et al.*, 1997). Above about 20 km, detrainment of material from the tropical reservoir is related to planetary wave activity. Thus, aerosol is preferentially transported into the winter hemi-

sphere. When QBO easterly winds overlie the equator, the aerosol reservoir remains relatively isolated from midlatitudes because the penetration of planetary waves into the tropics is inhibited, and removal of aerosols from the tropics occurs on a smaller scale along the periphery of the reservoir and just above the tropopause. Such was the case immediately following eruption of both El Chichón and Mt. Pinatubo (Trepte *et al.*, 1993). When QBO westerly winds are prevalent over the tropics, planetary waves can propagate deeper into the tropics and more easily transport aerosol poleward from the tropical reservoir. A large increase in aerosol loading from the El Chichón eruption was observed in the Northern Hemisphere during the autumn of 1982 after the equatorial stratosphere had made the transition to the westerly phase of the QBO (Pollack *et al.*, 1983).

The secondary circulation in the tropics associated with the QBO also has a strong influence on the dispersal of aerosols to higher latitudes (e.g., Plumb and Bell, 1982). In the westerly phase, there is equatorward flow above the shear layer, which leads to descent and a poleward spreading of conserved tracers below it. The descent of the QBO westerly shear in mid-1982 probably enhanced the transport of El Chichón aerosols into the Northern Hemisphere later that year (Hitchman *et al.*, 1994). The secondary circulation is reversed during the easterly QBO phase, so that aerosols tend to be lofted over the equator, as manifested by enhanced upward transport of Mt. Pinatubo aerosol over the equator during the last half of 1991.

Even though both El Chichón and Mt. Pinatubo are at approximately the same latitude, there was a distinct difference within the tropics in the movement of aerosols from these eruptions. In the case of El Chichón, most aerosols remained in the Northern Hemisphere (Pollack *et al.*, 1983; Stothers, 1996) whereas for Mt. Pinatubo, aerosols were rapidly transported south of the equator (Rosen *et al.*, 1994a; Godin *et al.*, 1996; Deshler *et al.*, 1997). Mt. Pinatubo simulations by Young *et al.* (1994) and Fairlie (1995) showed that meridional circulation resulting from aerosol-induced local heating caused the initial southward movement of SSA across the equator. However, significant aerosol heating was also noted after the eruption of El Chichón, even though no large-scale cross-equatorial drift of SSA was observed. Trepte *et al.* (1993) noted that strong QBO easterly winds above about 21 km over the equator might have inhibited transport into the Southern Hemisphere immediately after the eruption of El Chichón. In contrast, Mt. Pinatubo erupted when the easterly phase of the QBO was just descending through 25 km, and the absence of strong easterlies may have allowed significant amounts of material to be transported across the equator at lower altitudes.

A history of the dispersal of Mt. Pinatubo aerosol as measured by Northern Hemisphere ground-based lidars is shown in Figure 3-3 for the first 2 years following the eruption. The progression of SSA northward can be followed, and its intermittent nature in the first 6 months is obvious. The conservative nature of the volcanic aerosol between 6 and 9 months following eruption of Mt. Pinatubo has been illustrated by Borrmann *et al.* (1995), indicating that microphysical and vertical mixing processes were nearly completed by that time. This is apparent in the lidar data in Figure 3-3. The top of the aerosol layer is near 25 km, with the peak loading in the 16-22 km region. The altitude of the layer top and that of peak loading both decrease toward higher latitudes. Wintertime subsidence is clearly apparent in the northernmost measurements. A global view from SAGE II of the evolution of aerosol surface area from Mt. Pinatubo at two altitudes is shown in Figure 3-4. The relatively quiescent 6 years between eruption of El Chichón and Mt. Pinatubo are apparent, and within this period at 20 km the eruptions of Ruiz (in 1985) and Kelut (in 1990) can be seen. Ruiz erupted in the middle of the westerly phase of the QBO, which is favorable for the spread of material poleward in both hemispheres. Kelut erupted when strong easterlies were present at 20 km, and thus aerosol would be inhibited from crossing the equatorial region, leading to a preferential dispersal of the aerosol southward (Hitchman *et al.*, 1994). At 25 km the tropical stratospheric reservoir (20°S-20°N) is clearly evident (Trepte and Hitchman, 1992). The strength of the tropical barrier is illustrated by the confinement of the highest surface areas in the tropics even though Mt. Pinatubo was at the edge of the northern boundary. The preferential transport of aerosol to the winter hemisphere is also evident in Figure 3-4. The data indicate some hemispheric differences in the midlatitudes after 1994, as do balloonborne measurements (Deshler *et al.*, 1997).

3.3.1.2 Decay of Volcanic Aerosol

The decay of stratospheric volcanic aerosol proceeds at fairly well-defined rates. An exponential (e^{-1}) decay time of 1 ± 0.2 years generally characterizes the

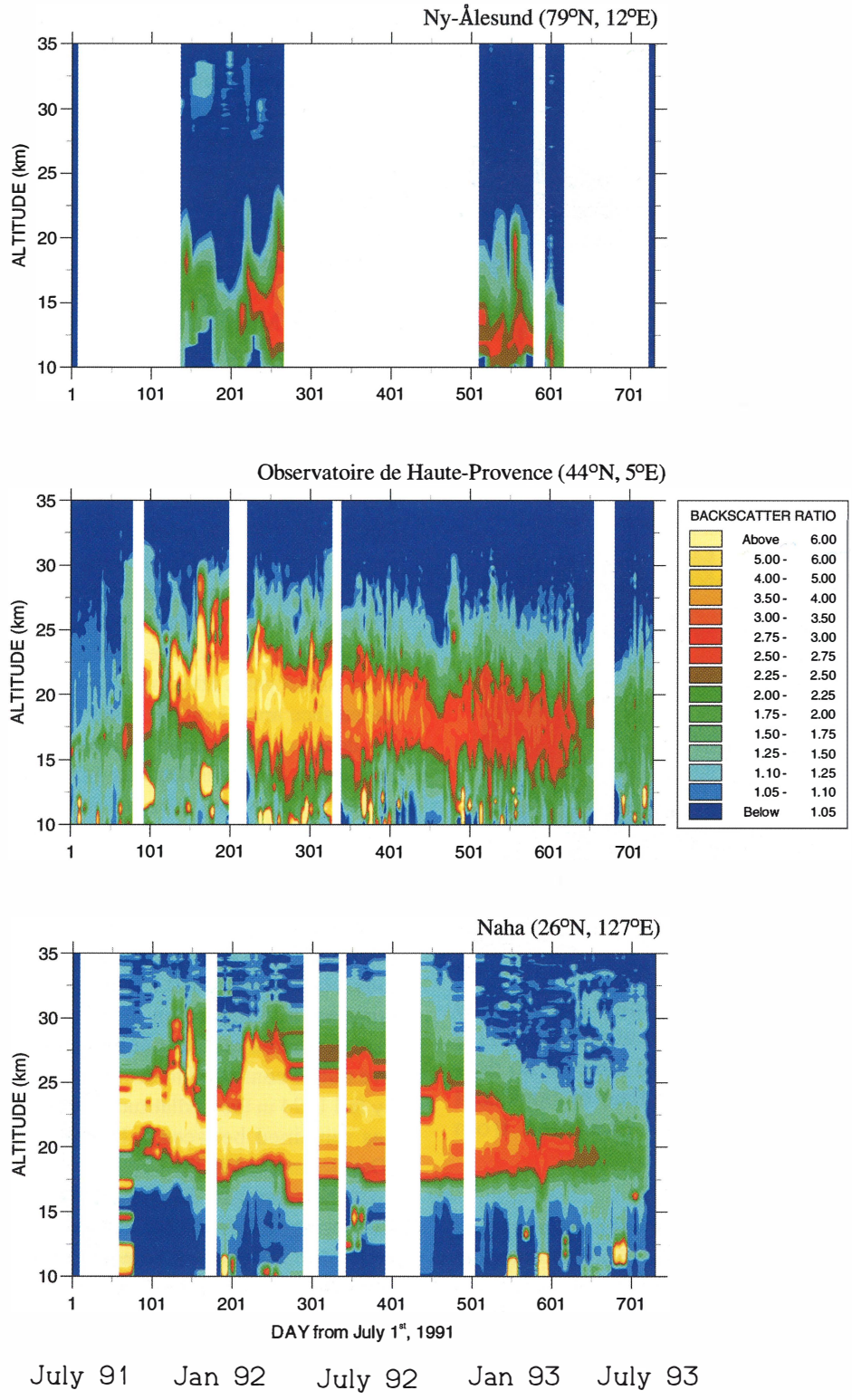

Figure 3-3. Time-height profiles of backscatter ratio from lidar measurements at Ny-Ålesund (79˚N), Observatoire de Haute Provence, France (44˚N), and Naha, Japan (26˚N).

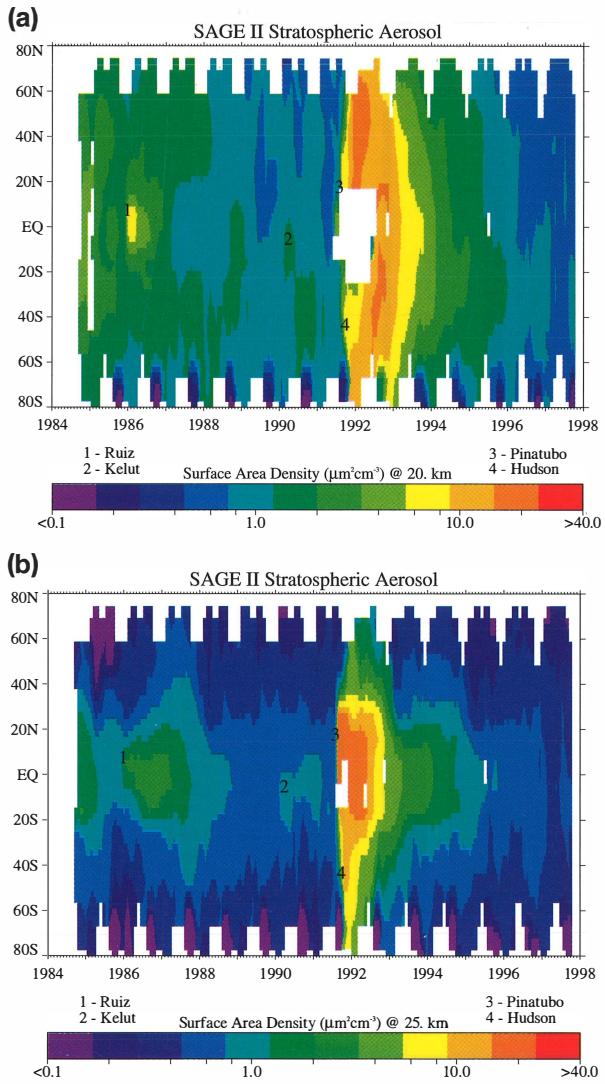

Figure 3-4. SAGE II aerosol surface area density as a function of time and latitude at altitudes of (a) 20 and (b) 25 km. White regions indicate no data are available. The latitude and time of significant volcanic events are noted. (Adapted from Thomason *et al.*, 1997a.)

behavior of any of several aerosol measurements during the first 3 years following the Mt. Pinatubo eruption: peak backscatter, peak mass, column backscatter, and column mass (Rosen *et al.*, 1994a; Jäger *et al.*, 1996; Barnes and Hofmann, 1997; Deshler *et al.*, 1997). The decay of the peak parameters is smoother than the decay of columnar quantities because the latter are more influenced by air mass transport, fluctuations in tropopause height, and stratospheric-tropospheric exchange (Rosen *et al.*, 1994a). The peak parameters reflect primarily sedimentation, are much less influenced by global- and synoptic-scale circulation after the initial mixing period, and are not influenced by fluctuations in tropopause height. Column backscatter measurements by Kent and Hansen (1998) show an e^{-1} time from September 1994 to December 1997 that was more than double (1.8 years) that observed during the immediate post-Pinatubo period (0.8 year). The decay of aerosol surface area at three altitudes in the northern midlatitudes following eruption of Mt. Pinatubo is shown in Figure 3-5. The nature of the decay curves and the time required to reach pre-eruption conditions are different at the three altitudes. At 25 km, there is a clear QBO signature, and average surface areas reached pre-Pinatubo values by early 1995, some 3.5 years after the eruption. The decay at 20 km is considerably smoother, but it took an additional year (until early 1996) to reach pre-eruption conditions. The record at 15 km is quite different, clearly showing seasonal changes, namely, increases in winter/spring and decreases in summer/fall. At this altitude, pre-Pinatubo surface areas were not reached until mid- to late 1996, more than 5 years after the eruption. The decay of aerosol surface area is on the order of 20-30% slower than the decay of backscatter or mass (Rosen *et al.*, 1994a; Jonsson *et al.*, 1996; Deshler *et al.*, 1997). Chazette *et al.* (1995) found the decay of integrated backscatter between 15 and 20 km to be on the order of 25% longer after Mt. Pinatubo than after El Chichón eruption. They attributed this slower decay to the higher lofting of particles following eruption of Mt. Pinatubo. Russell *et al.* (1996) showed that the stratospheric aerosol effective radius increased from 0.15 μm prior to the Mt. Pinatubo eruption, to a maximum near 0.55 μm one year later, then decreased to 0.45 μm by spring 1993. The effective radius continued to decrease to a value of <0.2 μm by fall 1994 in the midlatitudes of both hemispheres and has remained between 0.15 and 0.2 μm since then (Deshler *et al.*, 1997).

Number size distributions at 20 km for the first five springs following Mt. Pinatubo eruption are shown in Figure 3-6 and are compared with a pre-Pinatubo measurement, when the data were well represented by a unimodal lognormal distribution. After the eruption the data are represented with a bimodal lognormal distribution. The two modes of the distribution were initially quite narrow, and the median radius in the small-particle mode (r_1) increased by a factor of 2. In the next 3 years r_1 decreased, and the width (σ_1) in the first mode in-

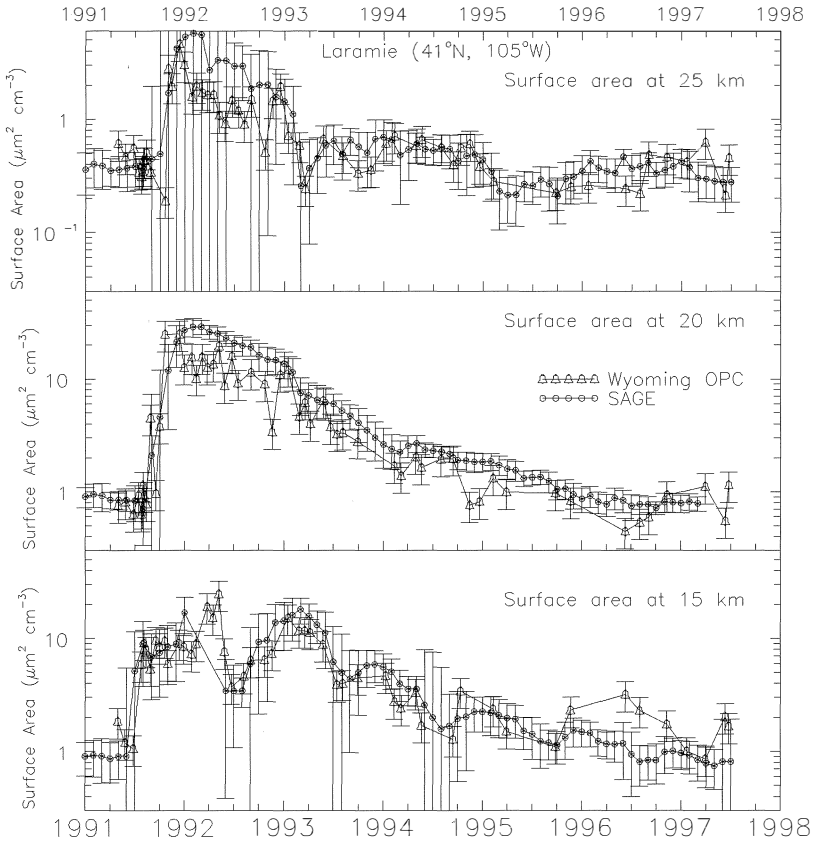

Figure 3-5. History of the evolution of aerosol surface area at 25, 20, and 15 km following the Mt. Pinatubo eruption. Surface areas estimated from balloonborne in situ optical particle counter (OPC) measurements above Laramie (41°N) and from SAGE II data in the 35°-45°N latitude band are shown. The error bars on the in situ data represent an uncertainty of 30%. The SAGE II error bars represent the standard deviation about the zonal median. (Adapted from Thomason *et al.*, 1997a.)

creased. The particle concentrations (N_1, N_2) and surface areas (A_1, A_2) shown for the springs of 1992 and 1993 compare favorably with ER-2 measurements by Jonsson *et al.* (1996). The second (large-particle) mode is well defined throughout the 5 years shown in Figure 3-6, preserving a quite similar shape. The primary change in the second mode is in the number concentration (N_2), which decreased steadily by about a factor of 5 per year. The second mode had almost disappeared by spring of 1997.

Quite similar decay rates have been observed for SSA from the El Chichón and Mt. Pinatubo eruptions (Rosen *et al.*, 1994a; Chazette *et al.*, 1995; Barnes and Hofmann, 1997), and from the decay at different latitudes for Mt. Pinatubo aerosol (Jayaraman *et al.*, 1995; Jäger *et al.*, 1996). These decay rates are also similar to that observed for the removal of strontium from the stratosphere (Fabian *et al.*, 1968). These similarities reflect the fact that the removal of SSA, once it is dispersed meridionally, is controlled by relatively steady and robust processes, such as gravitational settling and stratospheric-tropospheric exchange. The maximum stratospheric-tropospheric exchange of tracers is in the Northern Hemisphere spring (Holton *et al.*, 1995), which may explain the clear signature of a surface area minimum at 15 km in Figure 3-5 during that season each year. The temporal and vertical resolution required to capture stratospheric-tropospheric exchange processes in detail is provided by lidar, and several such studies have pointed out the influence of volcanic SSA on the upper troposphere (Menzies and Tratt, 1995; Sassen *et* al., 1995; Post *et al.*, 1996).

3.3.2 Background Aerosol

Since the discovery of the SSA layer in 1957 (Junge *et al.*, 1961) there has been much speculation about the stability of the layer and the source of the H_2SO_4 that is the primary component of the aerosol. The measurements by Junge *et al.* were made at the end of a lengthy period free of volcanic eruptions (Stothers, 1996), but were not extensive enough to establish a baseline. There are four periods in the modern (post-1970) measurement era when the influence of volcanic eruptions has been at a minimum: 1974, 1979, 1989 to early 1991, and the present (1998). Many studies have focused on these data

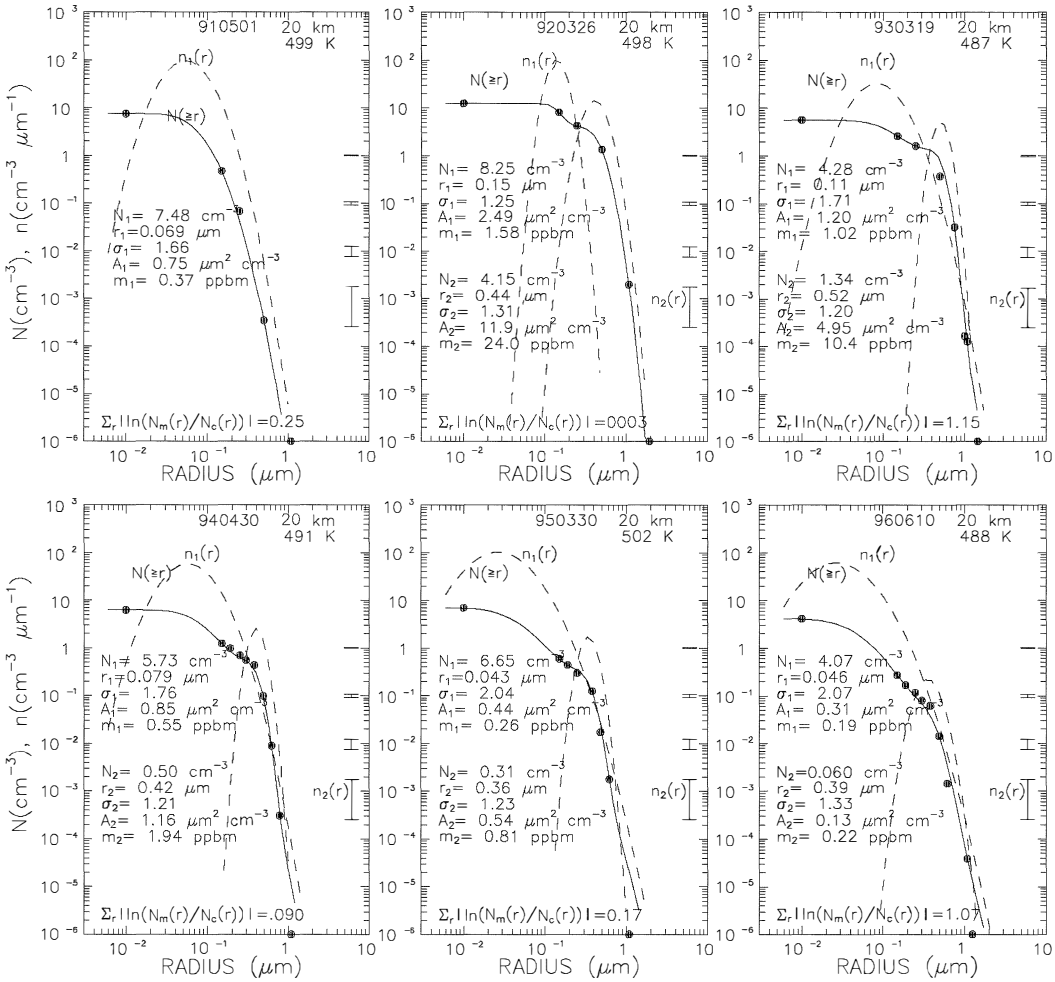

Figure 3-6. Unimodal/bimodal differential (*n*) and integrated (*N*) lognormal size distributions fitted to 1-km averaged particle counter measurements (solid circles) at 20 km above Laramie for the springs of 1991-1996. The parameters of the size distributions and the inferred surface area (*A*) and mass mixing ratio (*m*), assuming a composition of 65% H_2SO_4 by weight, are shown on the figure. Uncertainties in the concentration measurements are shown by the vertical bars on the right-hand side. The goodness of the fit is shown at the bottom as the sum of the log of the ratios of measured and calculated number concentration (N_m, N_c).

periods in an attempt to clarify the processes by which the background non-volcanic SSA layer is sustained and to explain the cause(s) for changes observed between the recent minimum periods.

In situ measurements at 41°N presented by Hofmann (1990a) showed an SSA increase of 30-50% between 1979 and 1989, a result corroborated by SAGE data at this latitude (Thomason *et al.*, 1997b). It was suggested that increased surface emissions of OCS or SO_2 (Hofmann, 1990a) or sulfur from aircraft exhaust (Hofmann, 1991) might be responsible for the observed SSA increase. Model results by Bekki and Pyle (1992) suggest that although aircraft may be a substantial source of sulfate below 20 km, the rise in air traffic from 1979 to 1989 was too small to account for the observed increase in SSA. More recent studies suggest also that the amount of stratospheric sulfur derived from OCS oxidation (Chin and Davis, 1995) is too small to sustain the observed minimum SSA loading. This led Chin and Davis to question whether the minimum SSA periods in the modern data record have been truly free of volcanic effects. Near-global SAGE II data, in fact, show that the 1989-1991 minimum period was influenced by the smaller volcanic eruptions of Nevado del Ruiz in 1985

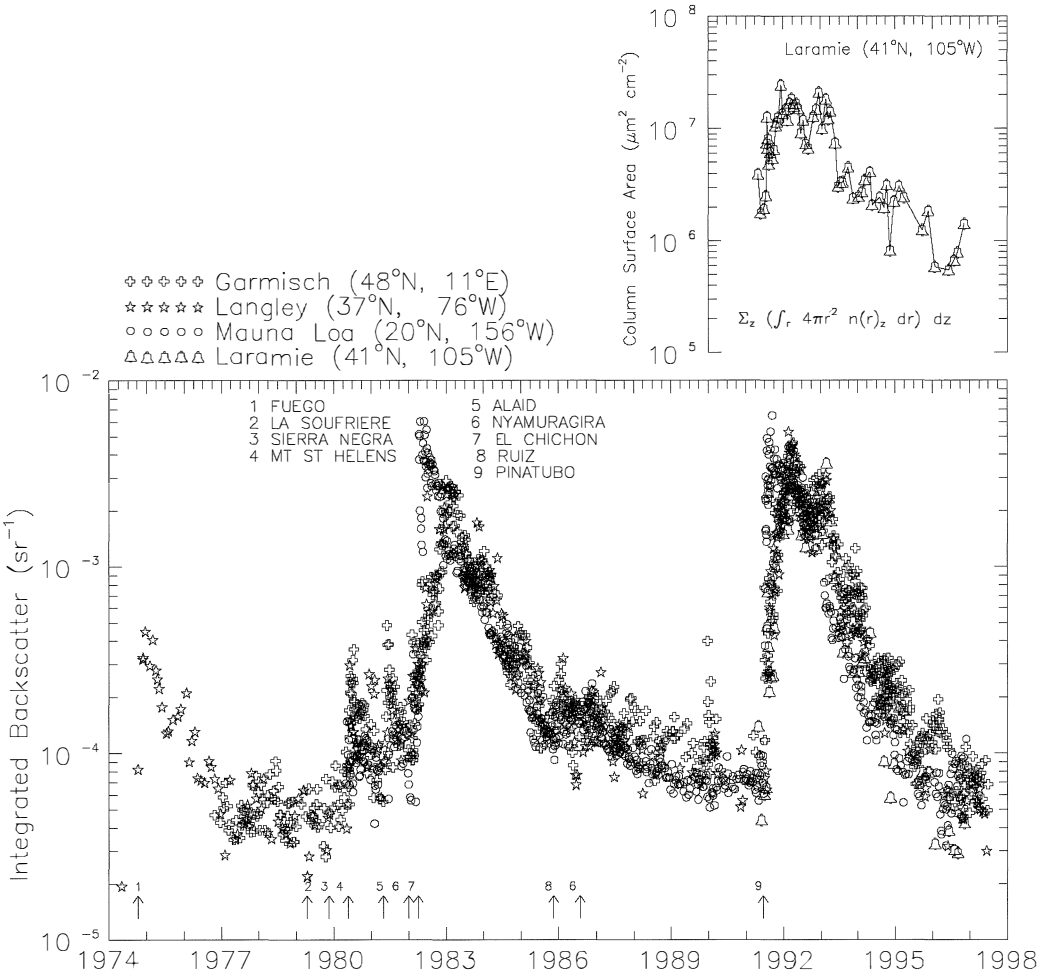

Figure 3-7. Integrated aerosol backscatter at a wavelength of 0.6943 μm from lidar measurements at Garmisch-Partenkirchen (48°N), NASA Langley (37°N), and Mauna Loa (20°N) for the period 1974-1998. Also shown for the period 1991-1997 is integrated aerosol backscatter calculated from size distributions fitted to in situ data above Laramie (41°N). The calculations assume particles with an index of refraction of 1.45. Also shown are column integrals of surface area from the 1991-1997 in situ data. The column integrals are from the tropopause to near 33 km for all the data.

and Kelut in 1990 (Thomason *et al.*, 1997b).

Figure 3-7 shows column stratospheric backscatter at the ruby wavelength (0.6943 μm) from ground-based lidar sites at Garmisch-Partenkirchen (48°N), NASA Langley (37°N), and Mauna Loa (20°N) for the period of 1974-1998. The Garmisch-Partenkirchen data for 1991-1998 were measured at a wavelength of 0.532 μm and converted to the ruby wavelength using balloonborne particle size information from Laramie. The figure also shows calculated column aerosol backscatter and surface area based on in situ size distribution data for 1991-1997 collected over Laramie. These SSA records are all in quite good agreement and show that levels in late 1997 were below pre-Pinatubo values, and are likely still decreasing. This means that any anthropogenic contribution must be less than previously estimated based on the observed 1979-1989 increase. Interpretation of the column data at low SSA levels is complicated by relatively large seasonal and QBO-related fluctuations. For example, in late 1996 column backscatter at Mauna Loa dropped as low as any observed in the previous 17 years, but increased in 1997 as the QBO changed phase (Barnes and Hofmann, 1997). Such a modulation is consistent with the tropical upper tropo-

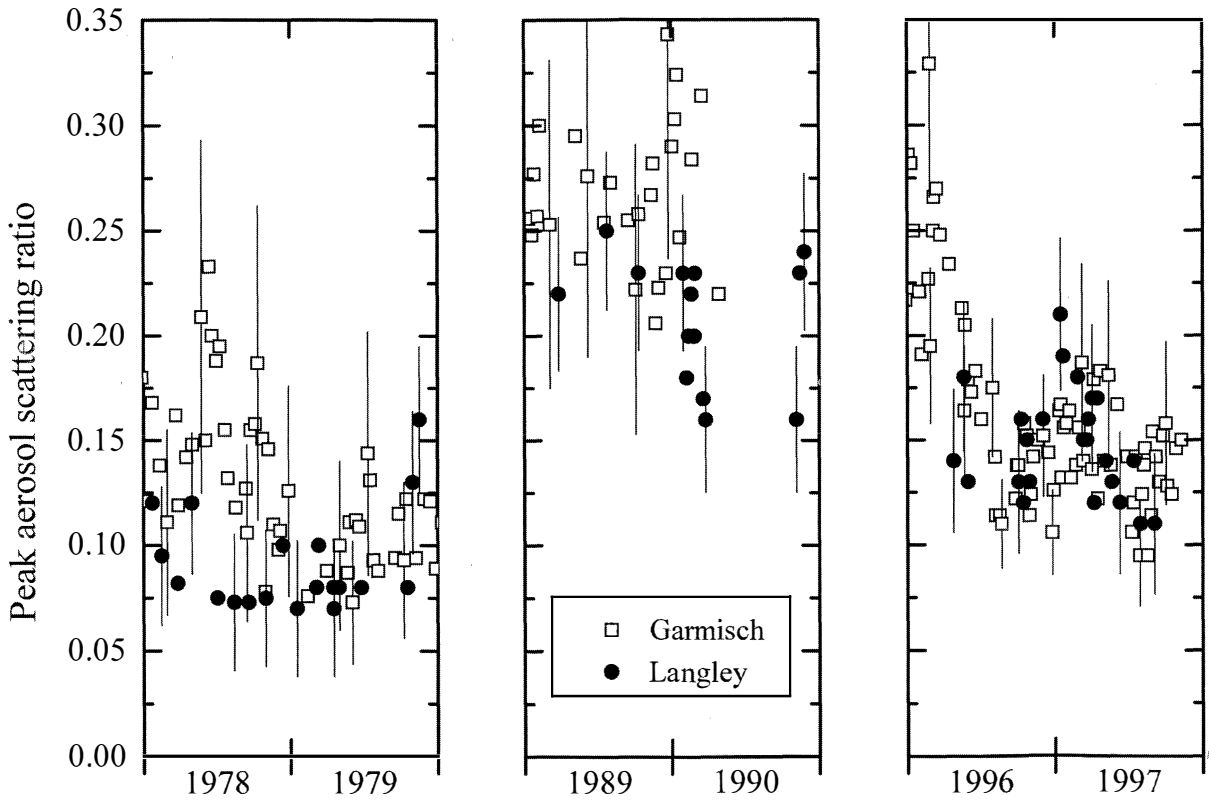

Figure 3-8. Peak aerosol scattering ratio at a wavelength of 0.6943 μm from lidar measurements at Garmisch-Partenkirchen (48°N) and NASA Langley (37°N) for 1978-1979, 1989-1990, and 1996-1997. Vertical bars are estimated uncertainties in representative measurements.

sphere being a source of CN (Brock *et al.*, 1995) and SO_2 (Weisenstein *et al.*, 1997). The midlatitude column measurements also show this SSA minimum, as well as the increase in 1997 with the QBO returning to a westerly phase. The midlatitude column data have a strong seasonal cycle, i.e., an increase and relative stability during winter and spring followed by a decrease in the summer and fall, that is closely tied to tropopause height. At very low SSA levels, column stratospheric backscatter can fluctuate by factors of 2 to 4 with season.

Long-term records have also been maintained of the peak aerosol scattering ratio, defined as the maximum value in a given lidar data profile of the ratio of aerosol backscatter to molecular backscatter. This quantity fluctuates less with season than do column integrals, and its uncertainty can be estimated quite easily. Figure 3-8 shows peak aerosol scattering ratio data (with representative estimated uncertainty bars) from Garmisch-Partenkirchen and Langley during 1978-1979, 1989-1990, and 1996-1997. Values in late 1997 were clearly lower than those observed in 1990, but were about 40% higher on average than those observed in early 1979. However, given the uncertainty in the individual measurements and the likelihood that SSA levels are continuing to decrease, the 1979-1997 difference must be viewed with caution at this time. Several more years of data uncorrupted by volcanic activity are required for determining if a stable background has been reached and for a more meaningful comparison with data from the 1979 minimum period.

3.4 PSC OBSERVATIONS

Observations of PSCs have been reported for more than a century (Stanford and Davis, 1974). Visual sightings have been mainly in northern Scandinavia during winter, where the clouds occasionally form in wave-like patterns of limited spatial extent when air parcels are lifted and cooled adiabatically over the Norwegian mountains. Due to the nearly monodisperse particle size

and the uniform variation in particle size across these clouds, wavelength-dependent scattering of incident sunlight may cause colorful appearances, giving rise to the name mother-of-pearl, or nacreous, clouds. Systematic satellite measurements later revealed that PSCs can occur on synoptic scales in both the Arctic and Antarctic when stratospheric temperatures fall below about 200 K (McCormick *et al.*, 1982).

3.4.1 Distinction between Types of PSCs

Chapter 7 shows that heterogeneous chlorine activation is controlled to first order by temperature and water vapor pressure, and not by detailed particle characteristics. However, in situations where there is not continued exposure to cold temperatures, such as in the Arctic, distinction and understanding of PSC types and details of particle size, composition, and phase are important.

Early ground-based and airborne lidar measurements indicated two distinct growth stages of PSCs (Iwasaka *et al.*, 1985; Poole and McCormick, 1988), giving rise to the classification into Type 1 PSCs, forming 2-6 K above the frost point (T_{ice}), and Type 2 PSCs, forming below T_{ice}. Lidar depolarization measurements in the Arctic later showed that Type 1 PSCs occur in at least two forms (Browell *et al.*, 1990; Toon *et al.*, 1990): Type 1a PSCs with low backscatter and high depolarization, corresponding to non-spherical, presumably solid particles; and Type 1b PSCs with high backscatter and low depolarization, suggesting spherical, presumably liquid particles (Carslaw *et al.*, 1994; Tabazadeh *et al.*, 1994). Type 2 PSCs have both high backscatter and high depolarization, corresponding to large ($r \geq 1$ μm) ice particles. Subsequent PSC lidar observations in both hemispheres have confirmed these classifications (Stefanutti *et al.*, 1991; Beyerle *et al.*, 1994; Adriani *et al.*, 1995; Stebel *et al.*, 1998; Shibata *et al.*, 1997; David *et al.*, 1998). This is demonstrated in Figure 3-9, which, for comparison, also includes SSA measurements, which exhibit both low backscatter and low depolarization. Table 3-1 summarizes the classification of particles observed in the winter polar stratospheres. Similar classifications of PSC particles have also been obtained from in situ backscatter ratio and color index measurements by balloonborne backscattersondes (Larsen *et al.*, 1997; Rosen *et al.*, 1997).

However, not all winter stratospheric particle observations can be categorized so narrowly. During strong mountain-wave-induced cooling, large particles, presumably Type 2 PSCs, have been observed at temperatures more than 3 K above T_{ice} (Deshler *et al.*, 1994a). Other observations suggest that a nitrate coating could prevent large ice particles from subliming at these elevated temperatures (Gandrud *et al.*, 1990; Wofsy *et al.*, 1990; Goodman *et al.*, 1997). At temperatures above T_{NAT}, the ubiquitous SSA is observed by lidar. The observations show large variability in backscatter due to varying aerosol mass loading after volcanic eruptions, but mostly exhibit low depolarization ratios, indicating spherical liquid particles. However, depolarizing and presumably small particles have occasionally been measured by lidars at temperatures above T_{NAT} (Adriani *et al.*, 1995; Stefanutti *et al.*, 1995; Stein *et al.*, 1995; Nagai *et al.*,

Table 3-1. Classification of stratospheric particle types, based on 0.532-μm lidar backscatter ratios and volume depolarization (David *et al.*, 1998)[1].

Particle type	Background aerosol	Volcanic sulfate aerosol	Type 1a PSC	Type 1b PSC	Type 2 PSC
Backscatter ratio	< 1.2	> 1.2	< 2	> 2	>2
Depolarization, %	<~ 1.5	<~ 1.5	>~ 1.5	<~ 1.5	10-50

[1] The backscatter ratio is defined here as $(B_p+B_m)/B_m$ where B_p and B_m are the particulate and molecular volume backscatter coefficients, respectively. The depolarization ratio is defined as the ratio between the total volume backscatter coefficients in the parallel and perpendicular planes relative to the polarization plane of the emitted laser beam.

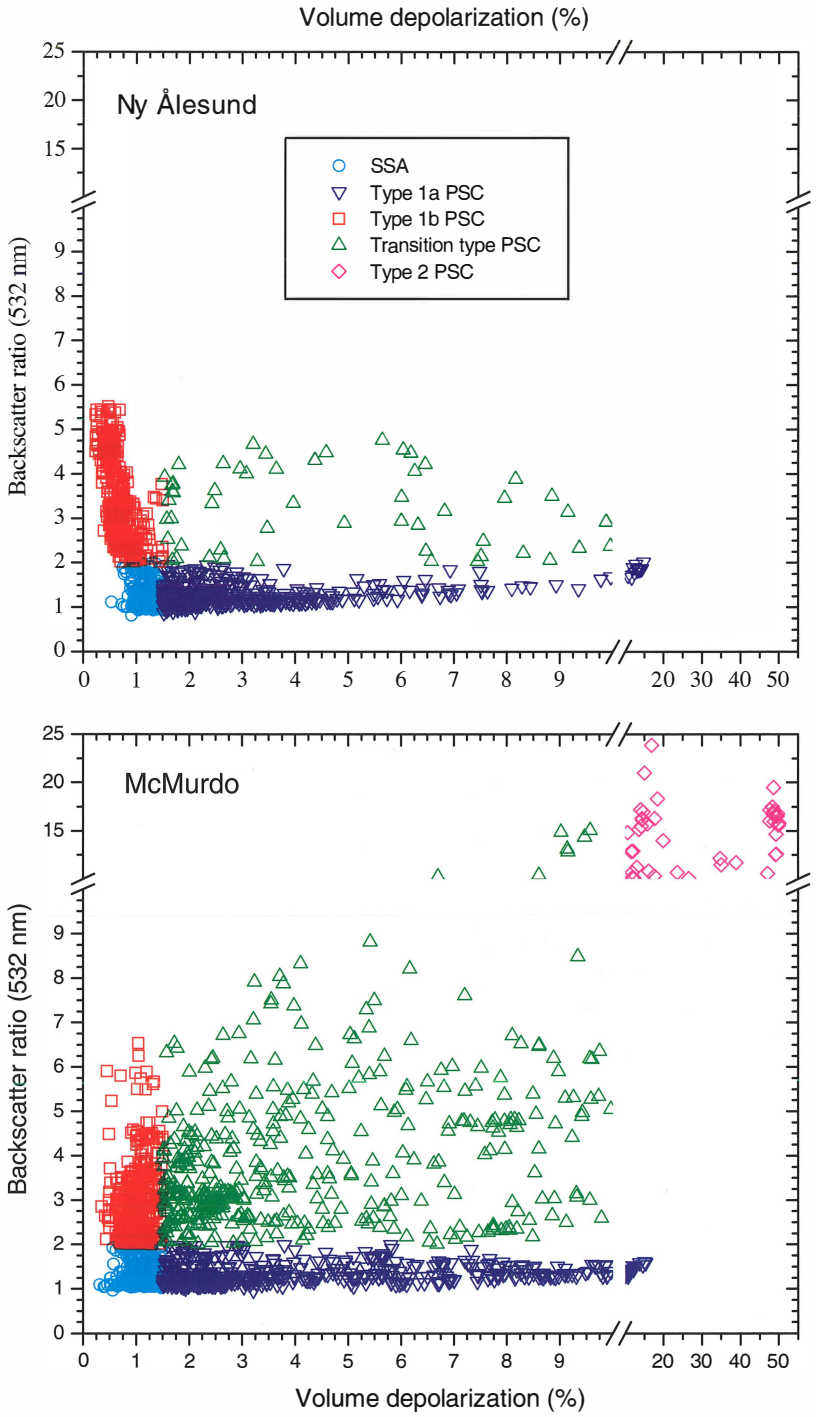

Figure 3-9. Scatter plots of 0.532-μm backscatter ratio versus volume depolarization from Arctic measurements at Ny-Ålesund, Spitsbergen, (upper panel) and Antarctic measurements at McMurdo (lower panel), illustrating the grouping of different particle types (classified as in Table 3-1) observed in the polar winter stratosphere. Note the changes of scales on the axes. The Arctic data points are used again in Figure 3-11 to show the temperatures at which the observations were made.

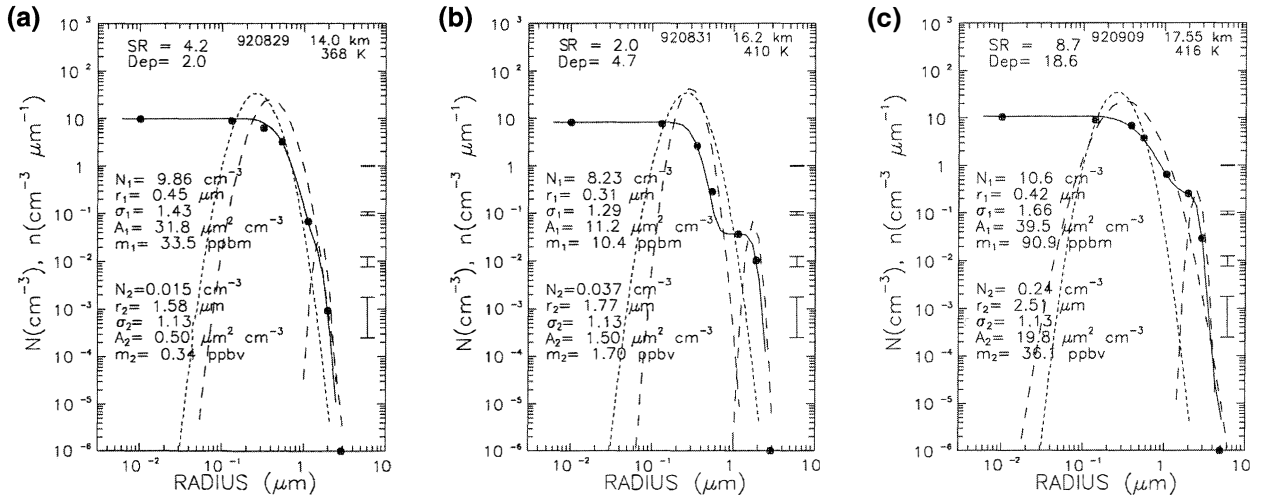

Figure 3-10. Example bimodal lognormal size distributions fitted to particle counter measurements (solid circles) in: (a) a non depolarizing PSC; (b) a depolarizing PSC with moderate scattering ratio; and (c) an ice cloud with high depolarization and high scattering ratio. The two differential distributions (long dashes) and the cumulative distribution (solid line) are shown in each panel. The constant unimodal curve (short dashes) in each graph is representative of the size distribution of SSA at the time of these PSC measurements. The parameters of each lognormal size distribution and the inferred surface area and mass are shown on the figures, as are the depolarization (Dep) and scattering ratios (SR) measured by lidar at the time of these in situ measurements. Uncertainties in the concentration measurements are shown by the vertical bars on the right-hand side. Refer to Figure 3-6 and Section 3.3.1.2 for definitions of symbols used in the figure legend.

1997), perhaps indicating solid remnants of previously formed PSC particles.

Because winter temperatures are generally lower in the Antarctic than the Arctic, Type 2 PSCs form much more frequently in the Southern Hemisphere. However, Type 2 PSCs have been observed by lidar and satellite in the Arctic, both under synoptic-scale cooling (McCormick *et al.*, 1990; Pitts *et al.*, 1990) and mountain-wave-induced cooling to below T_{ice} (Müller *et al.*, 1995; David *et al.*, 1997).

3.4.2 Measurements of PSC Characteristics

Aerosol depolarization measurements by lidar have provided the best indicator for non-spherical and thereby presumably solid particles in the stratosphere. In order to derive other PSC characteristics from remote sensing data, the refractive index of PSC particles of different composition must be known. Combinations of size distributions measured by optical particle counters and single-wavelength lidar observations have been used to estimate the real part of the refractive index (m) for PSC particles (Adriani *et al.*, 1995). At a wavelength of 0.532 μm, estimated values are $m = 1.42 \pm 0.04$ for NAT, $m = 1.39 \pm 0.03$ for STS (varying directly with temperature as derived from model calculations and multi-wavelength lidar measurements (Luo *et al.*, 1996; Beyerle *et al.*, 1997; Wedekind *et al.*, 1997), and $m = 1.32 \pm 0.01$ for Type 2 PSCs, as expected for ice.

PSC particle size distributions have been measured in situ by several instruments: the airborne forward scattering spectrometer probe (FSSP-300) and multi-angle aerosol spectrometer probe (MASP) (Ferry *et al.*, 1989; Dye *et al.*, 1992, 1996), airborne wire impactors (Goodman *et al.*, 1989, 1997), and balloonborne optical particle counters (Hofmann, 1990c; Hofmann *et al.*, 1990; Rosen *et al.*, 1990; Hofmann and Deshler, 1989, 1990, 1991; Deshler *et al.*, 1991, 1994a, 1994b; Deshler and Oltmans, 1998; Adriani *et al.*, 1992, 1995). Examples of typical PSC size distributions are shown in Figure 3-10. Unimodal Type 1 PSC distributions, with mode radii from 0.3 to 0.5 μm and representing a large fraction of the available condensation nuclei, are generally observed during faster synoptic cooling (4-10 K day^{-1}; Deshler *et al.*, 1991; Beyerle *et al.*, 1994; Adriani *et al.*, 1995). These particles have low depolarization, associated with Type 1b PSCs. In

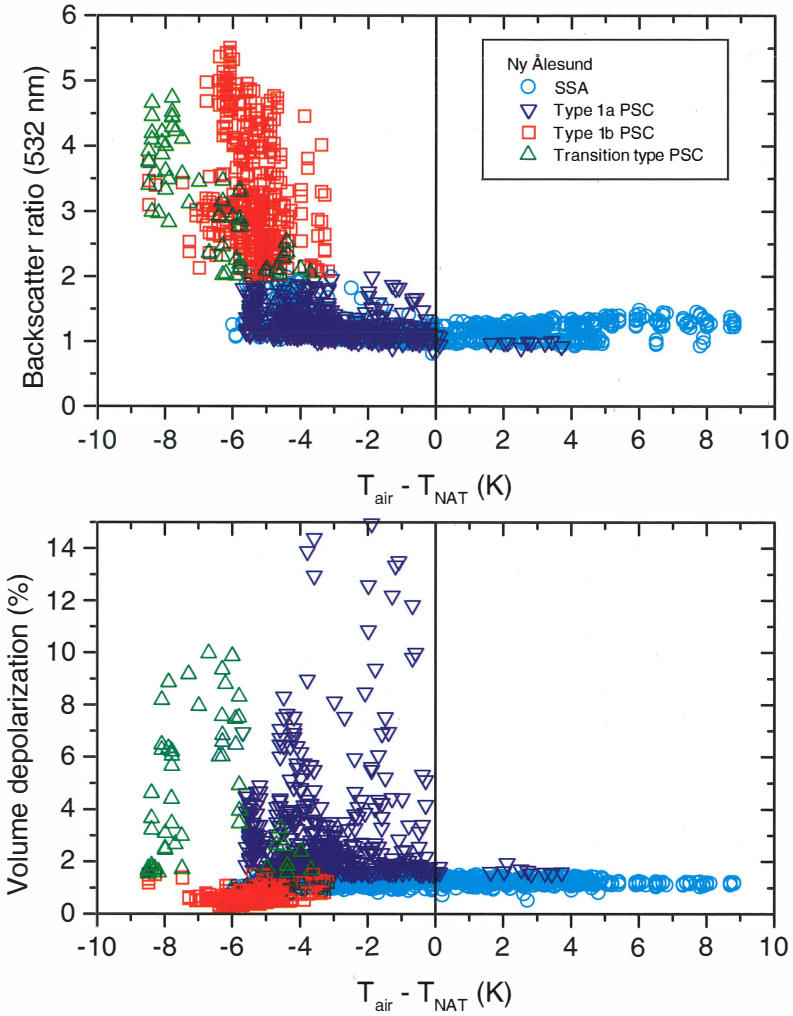

Figure 3-11. Scatter plots of aerosol backscatter ratio (upper panel) and volume depolarization (lower panel) versus the difference between ambient air temperature T_{air} and T_{NAT} from the Arctic lidar observations as shown in Figure 3-9. Type 1b PSCs show a characteristic sharp increase in backscatter ratio at roughly 3-4 K below T_{NAT}, as expected for STS particles (upper panel), whereas Type 1a PSC are observed at all temperatures below T_{NAT} (lower panel). The transition-type PSC particles are observed at temperatures approaching the ice frost point at roughly 7 K below T_{NAT}. T_{NAT} was estimated by assuming a high-latitude Northern Hemisphere LIMS (Limb Infrared Monitor of the Stratosphere) HNO_3 profile along with 4.6 ppm H_2O, and ambient air temperatures were obtained from daily radiosonde measurements.

bimodal Type 1 PSC size distributions, the large-mode radii are around 1.5-2.5 μm, and the large size mode typically represents less than 1% of the available condensation nuclei. These particles are observed during slower synoptic cooling (1-3 K day^{-1}; Beyerle *et al.*, 1994; Adriani *et al.*, 1995), sometimes forming in thin layers, and the particles have large depolarization, associated with Type 1a PSC. Type 2 PSC particles captured in situ have been predominantly solid and hollow columns and hexagonal plates, with sizes on the order of 5-50 μm and number concentrations of (0.5-5) × 10^{-4} cm^{-3} (Goodman *et al.*, 1989).

The first in situ Antarctic PSC measurements were obtained in mid- to late winter 1987; these indicated that the clouds could be composed of NAT (Fahey *et al.*, 1989). Observed size distributions are often bimodal

(Type 1a) (Hofmann and Deshler, 1991; Deshler *et al.*, 1991). Later observations from the Arctic revealed that PSCs often do not form until high supersaturation with respect to NAT is reached, indicating another composition of the particles (Rosen *et al.*, 1989; Schlager *et al.*, 1990). This was particularly the case for PSCs with a unimodal size distribution (Type 1b) where a large fraction of the condensation nucleus population undergoes particle growth (Dye *et al.*, 1990b; Hofmann *et al.*, 1990). From particle volumes derived from size distributions measured with the FSSP, it appeared that SSA could remain in the supercooled liquid state to very low temperatures (down to at least 193 K) and over large regions of the Arctic. The main increase in Type 1 PSC particle volume was observed at temperatures 3-4 K below T_{NAT} (Dye *et al.*, 1992). In Figure 3-1 measurements of particle volumes from the NASA ER-2 flight on 24 January 1989 were explained in terms of STS solution droplets in equilibrium with the ambient HNO_3 and H_2O vapor (Drdla *et al.*, 1994; Tabazadeh *et al.*, 1994; Carslaw *et al.*, 1994, 1995). This explanation is based on thermodynamic models for electrolytic solutions. Ground-based lidar (Beyerle *et al.*, 1997; David *et al.*, 1998), satellite (Taylor *et al.*, 1994; Massie *et al.*, 1997), balloonborne backscatter sonde (Larsen *et al.*, 1997; Rosen *et al.*, 1997), and airborne in situ (Dye *et al.*, 1996; Del Negro *et al.*, 1997) data have provided further evidence that Type 1b PSCs are associated with an STS composition. By relating the lidar measurements of PSC particles to the difference between the air temperature and T_{NAT}, as shown in Figure 3-11, a sharp increase in aerosol backscatter for Type 1b PSCs is observed at temperatures 3-4 K below T_{NAT}, as expected from STS droplets. Also, infrared spectroscopic measurements of PSCs have indicated an STS composition (Toon and Tolbert, 1995), and satellite observations have shown that gas-phase HNO_3 is depleted at temperatures where STS droplets could initially be expected to form (Santee *et al.*, 1998). Hence, there is substantial observational evidence that Type 1b PSCs have an STS composition.

Type 1a PSC particles are observed at all temperatures below T_{NAT} (cf. Figure 3-11), indicating a NAT composition for at least some of the observations (Larsen *et al.*, 1996, 1997; Rosen *et al.*, 1997; David *et al.*, 1998), in agreement with earlier observations from Antarctica (Fahey *et al.*, 1989). Measurements of low column abundances of gas-phase HNO_3 by Höpfner *et al.* (1996) have also indicated the existence of equilibrium NAT particles in the Arctic. The smooth, compact relationship between particle volume and temperature characteristic of STS droplets (Figure 3-1) is not present in all observations (Dye *et al.*, 1992, 1996; Tabazadeh *et al.*, 1995). Figure 3-12 shows particle counter measurements made on the ER-2 aircraft on 16 January 1989 in the Arctic, similar to those already shown for 24 January 1989 in Figure 3-1a. On the basis of simultaneous in situ measurements of NO_y and particle volume, Tabazadeh and Toon (1996) inferred the composition of a subset of PSC particles observed on 20 January 1989 to be a metastable water-rich HNO_3/H_2O solid phase. They named these particles Type 1c PSCs and suggested them as possible precursors of more stable NAT or nitric acid dihydrate (NAD) Type 1a PSCs. Presently, it is uncertain if the transition-type PSC seen in Figures 3-9 and 3-11 is indicative of Type 1c PSCs. For this same series of ER-2 flights, measurements that deviate from the compact STS curve have also been interpreted as not fully developed NAT clouds since the equilibrium times of NAT particles are relatively long (Peter, 1997). The various panels of Figure 3-12 are explained in detail in Chapter 7, Section 7.2.2.

3.4.3 Spatial and Short-Term Variability of PSCs

Many observations suggest that PSCs can exist on synoptic scales, therefore providing a large area through which air parcels can be processed. In addition, mesoscale temperature fluctuations caused by gravity waves or mountain waves can cause PSCs to form on smaller spatial scales.

3.4.3.1 Synoptic-Scale PSC Formation

Synoptic-scale PSCs located outside typical mountain wave regions have been observed by airborne lidar and in situ sensors (e.g., Browell *et al.*, 1990; McCormick *et al.*, 1990; Dye *et al.*, 1992), and by ground-based lidars (e.g., Adriani *et al.*, 1995; Stebel *et al.*, 1998; Shibata *et al.*, 1997; David *et al.*, 1998) and backscattersondes (e.g., Rosen *et al.*, 1993; Larsen *et al.*, 1997).

Tabazadeh *et al.* (1995) analyzed the temperature histories of a subset of in situ measurements of synoptic-scale PSCs encountered by the ER-2 in January 1989 (Dye *et al.*, 1992). This analysis showed that PSC particles observed on 24 and 25 January that had STS properties (i.e., Type 1b PSCs; cf. Figure 3-1a) had experienced a relatively fast cooling from above the sulfuric acid tetrahydrate (SAT) melting temperature. Other PSC data, from the same series of flights, that deviated

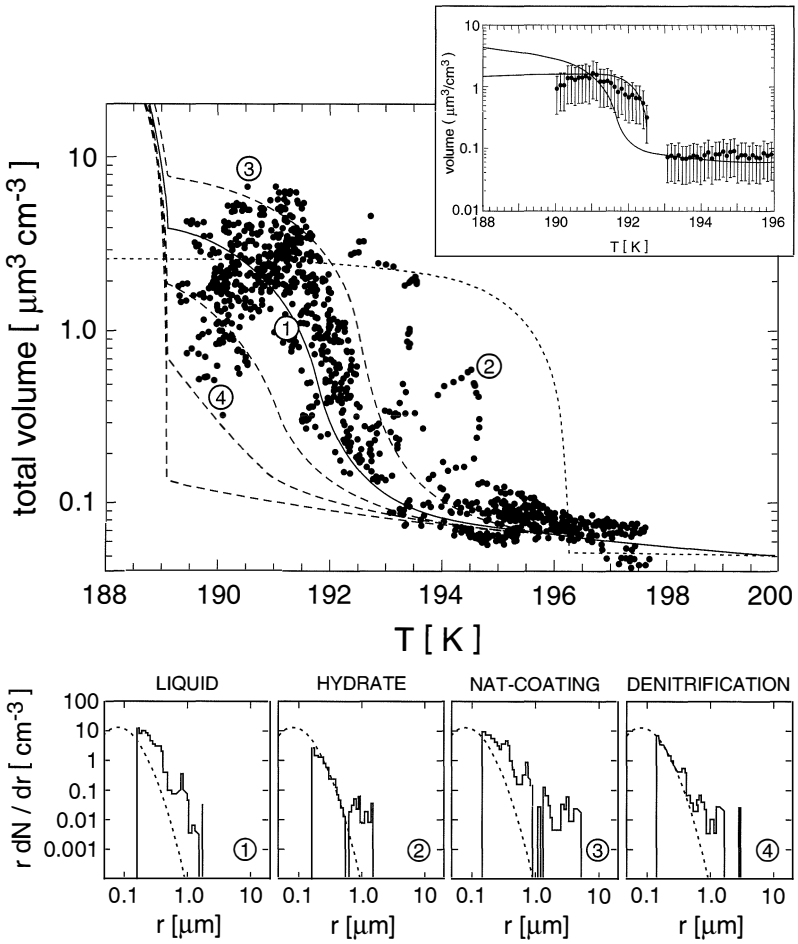

Figure 3-12. Upper large panel: Total particle volume observed by Dye *et al.* (1992) under conditions as in Figure 3-1, but on 16 January 1989. All calculations assume 5 ppm H_2O. Solid line: STS droplets for 10 ppb HNO_3. Dashed lines (top to bottom): STS droplets for 20, 5, 2, and 0 ppb HNO_3. Dotted line: NAT for 10 ppb HNO_3. Lower small panels: Examples of the measured particle size distribution (cases 1-4 refer to the corresponding points in the upper panel). (1) STS droplets at 193.3 K; (2) nonequilibrium particles at 194.8 K (Type 1a); (3) large particles at 190.5 K tentatively identified as NAT-coated ice particles; (4) particles under strongly denitrified conditions at 190.2 K. (Adapted from Peter, 1997.) Insert: Average values and standard deviations of reduced dataset (time window and $r < 2$ μm) interpreted thermodynamically as a new cloud type (Type 1c). (Adapted from Tabazadeh and Toon, 1996.)

from the compact STS curve were not exposed to SAT melting and had experienced cooling/warming cycles. Tabazadeh *et al.* (1995) explained this in terms of the formation of numerous small Type 1c particles prior to the aircraft encounter (see Section 3.4.2), whereas Peter (1997) argued that the bimodal character of the particle distribution would point toward Type 1a particles possibly mixed into a Type 1b cloud. A further analysis of airborne lidar observations by Tabazadeh *et al.* (1996) concluded that air masses must be exposed to synoptic temperatures below T_{NAT} for 1 day or more in order for synoptic-scale Type 1a PSCs to form.

Similar analyses of synoptic-scale PSC observations by ground-based lidar in Antarctica (Adriani *et al.*, 1995) and by backscattersondes in the Arctic (Larsen *et al.*, 1996, 1997) also suggested that most liquid Type 1b

PSC particles are observed during fast synoptic cooling, shortly (<1 day) after entering a cold region. Solid Type 1a PSCs, in contrast, were observed when temperatures had been below T_{NAT} for a longer time during both synoptic cooling and heating.

3.4.3.2 Mesoscale PSC Formation

Gravity waves can cause mesoscale temperature fluctuations of moderate amplitude (~4 K peak-to-peak) that are ubiquitous and must be superimposed on synoptic-scale air parcel trajectories (Murphy and Gary, 1995). Even larger perturbations (>20 K peak-to-peak) with cooling rates greater than 50-100 K h^{-1} can be encountered in mountain waves (Volkert and Intes, 1992), causing the development of different PSC characteristics on synoptic and regional spatial scales. PSC formation in mountain lee waves has been observed extensively from Kiruna, Sweden, by ground-based and airborne lidars and balloonborne optical particle counters. Strong temperature perturbations, induced by adiabatic lifting of air parcels over the Norwegian mountains and superposed on low synoptic-scale temperatures, clearly influence the cloud formation, as observed by airborne lidars flying parallel to the air flow (e.g., Godin *et al.*, 1994). The temperature may approach or go below T_{ice} for relatively short periods, causing peculiar PSC features. Particle microlayers with vertical thickness of 75-300 meters have been observed in the Arctic, in which a small fraction (<1%) of the available condensation nuclei have grown into large (2-3 μm) solid particles (Hofmann and Deshler, 1989; Hofmann, 1990c; Stein *et al.*, 1995). Some data in these microlayers are consistent with a NAT particle composition. Other large particles (up to 5 μm) observed by Deshler *et al.* (1994a) and constituting a larger fraction of the available condensation nuclei must have been composed mainly of ice (taking into account their large size), even though temperatures were well above T_{ice}. Also thin layers of Type 2 PSC, surrounded by thick layers of liquid Type 1b PSC, have been observed (David *et al.*, 1997).

Figure 3-13 gives an impressive quasi-Lagrangian view of PSC formation in lee waves as observed by airborne lidar crossing the mountains near Kiruna in a direction almost parallel to the stratospheric wind. Strong gravity wave perturbations are clearly visible in the particle backscatter (upper panel). These perturbations indicate temperature fluctuations of up to 13 K peak-to-peak with cooling/heating rates of more than 100 K h^{-1}. Apparently, two distinct and not well understood formation processes of solid particles, identified by large depolarization ratios (lower panel), are captured by these measurements (Carslaw *et al.*, 1998). Between 17°E and 18°E, numerous Type 2 PSC ice particles seem to form directly from liquid Type 1b PSCs. Slightly downstream of this region, liquid PSC particles are again observed. Farther downstream, east of 22°E, a small number of depolarizing (solid) particles with low backscatter ratios (Type 1a PSC) appear to form gradually out of the background aerosol population. This indicates that freezing processes in connection with mountain-wave-induced ice clouds could represent an additional mechanism for Type 1a PSC formation (Meilinger *et al.*, 1995).

3.4.4 Seasonal Evolution and Hemispheric Differences

3.4.4.1 Temperature Conditions

In the Arctic, where climatological stratospheric temperatures do not fall below the PSC formation thresholds, the clouds mainly form and disappear repeatedly in connection with transient, synoptic-scale cold outbreaks (Taylor *et al.*, 1994; Pawson *et al.*, 1995) and in mountain wave regions. In addition, individual air parcels often experience temperatures above the SAT melting temperatures during winter, whereby any remnants of solid PSC particle formation would presumably disappear. Therefore, throughout the Arctic winter, temperatures hover around the threshold for PSC formation, and the clouds are generally observed shortly after they initially form, often in liquid or perhaps metastable phases.

Over Antarctica, climatological temperatures are lower than T_{NAT} for several months and often fall below T_{ice} as well. PSCs occur continually throughout the winter and, hence, can be observed well after their initial formation period. Individual PSC particles presumably exist for longer periods, which increases the probability of freezing into stable NAT or ice particles. The lower temperatures and longer lifetime of individual PSC particles favor the formation of relatively large particles. This, together with a longer PSC season, leads to more efficient denitrification and dehydration by particle sedimentation, as compared to conditions in the Arctic. Hence, climatologically different temperatures may give rise to hemispheric differences in particle properties and seasonal PSC evolution, and thereby to differences in heterogeneous processing leading to ozone depletion.

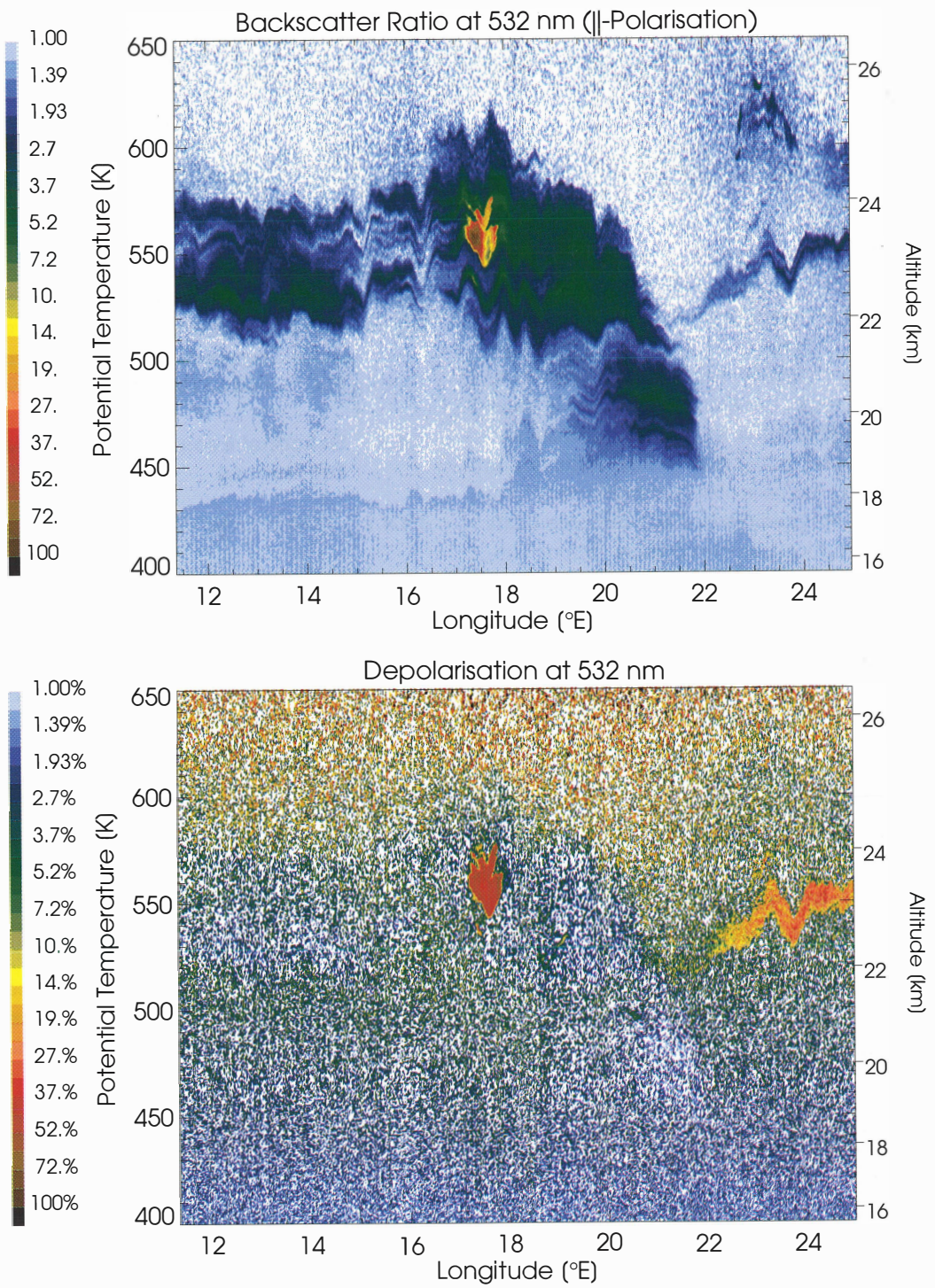

Figure 3-13. Altitude/longitude plot of airborne lidar observations from the German Transall aircraft on 15 January 1995 over the Norwegian mountains west of Kiruna, showing 0.532-μm aerosol backscatter ratio (upper panel) and depolarization (lower panel). The wind direction was from west to east (left to right in the figure). (Adapted from Carslaw *et al*., 1998.)

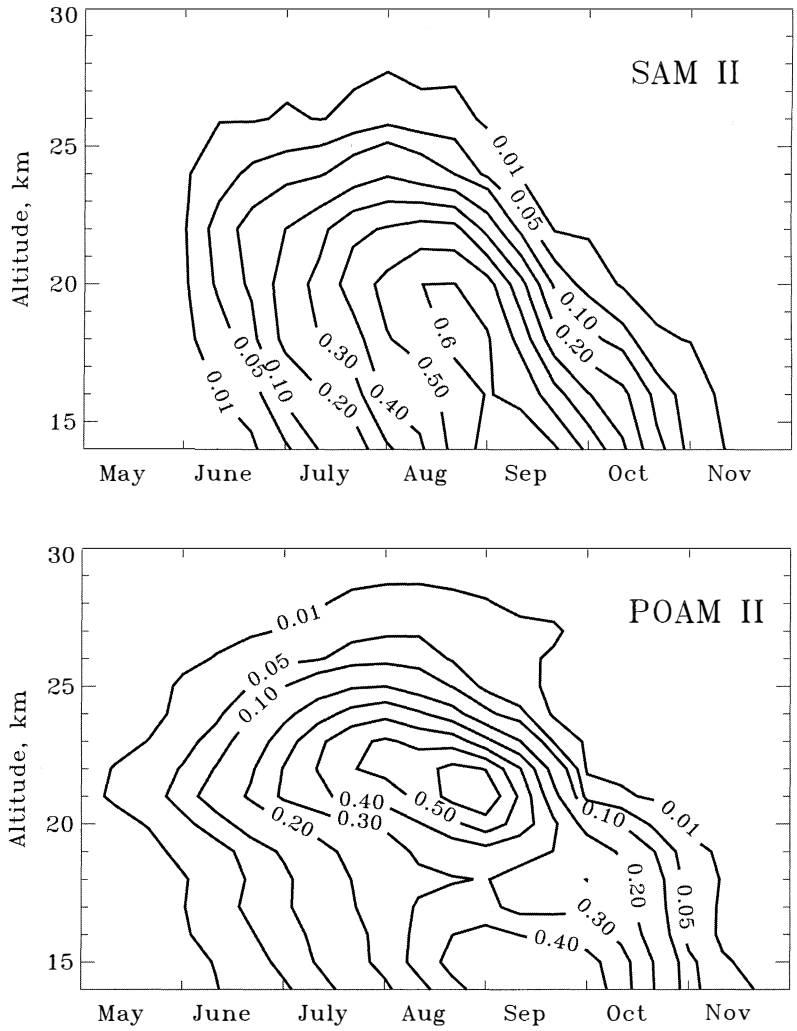

Figure 3-14. Zonally averaged PSC sighting probabilities for the Antarctic from measurements by SAM II for 1979-1989 (upper panel) and POAM II for 1994-1996 (lower panel). (Adapted from Poole and Pitts, 1994; and Fromm *et al.*, 1997.)

3.4.4.2 PSC Climatology

A PSC climatology was developed from more than 10 years of measurements by the Stratospheric Aerosol Measurement (SAM) II satellite instrument (Poole and Pitts, 1994). The frequency of occurrence of Antarctic PSCs observed by CLAES in 1992 generally agreed with this climatology (Mergenthaler *et al.*, 1997). PSC observations in both hemispheres were also made more recently (October 1993-November 1996) by POAM II (Fromm *et al.*, 1997). Figure 3-14 shows SAM II and POAM II zonally averaged PSC sighting probabilities for the Antarctic. Both datasets show Antarctic PSCs forming from mid-May until early November, with sighting probability increasing throughout the winter to a peak of about 60% in mid to late August. There is a downward trend in the altitude of peak sighting probability related to the seasonal descent of the altitude of coldest temperature, a feature also noted in lidar measurements (David *et al.*, 1998). SAM II and POAM II Arctic PSC sighting probabilities (not shown) differ in an absolute sense, primarily because of the difference in latitude sampling of the two instruments. However, the Arctic data records are qualitatively similar, showing that PSCs occur there much less frequently and over a shorter time period (from early December to mid March) than in the Antarctic (Poole and Pitts, 1994).

Poole and Pitts (1994) noted that PSC existence temperatures inferred from SAM II data were nearly constant throughout the winter season in the Arctic, whereas a gradual lowering of existence temperatures was inferred over Antarctica from June through September, indicating a systematic removal of HNO_3 and H_2O by denitrification and dehydration in that region. The

existence temperatures in the early winter season in both hemispheres were close to the expected NAT equilibrium temperatures. On the other hand, gas-phase HNO_3 measurements by the Microwave Limb Sounder (MLS) instrument (Santee *et al.*, 1998) show early-winter HNO_3 condensation beginning at roughly 3 K below T_{NAT}. This indicates that STS PSC particles were formed initially. Later in the season, HNO_3 concentrations approached the equilibrium levels for NAD (or NAT).

3.4.4.3 Effects of Volcanic Loading on PSC Formation

Large concentrations of volcanic SSA were observed to influence PSC formation in the years following the 1991 Mt. Pinatubo eruption. Antarctic measurements by Deshler *et al.* (1994b) showed that PSCs formed in the volcanic layer had numerous small particles ($r <$ 0.5 μm) and essentially no particles with $r > 2$ μm, and that surface areas increased by a factor of 4 to 6 relative to the surrounding SSA. At altitudes above the volcanic layer, particles with $r \approx$ 2-3 μm were observed, as had been the usual case in Antarctica prior to the eruption. Lidar observations show that most of the PSCs formed near the peak in SSA backscatter and at lower altitudes in the first years after eruption of Mt. Pinatubo. The larger volcanic aerosol loading apparently led to increased Type 1b PSC formation at higher temperatures, compared to pre-volcanic conditions (David *et al.*, 1998). Satellite measurements also show a more pronounced HNO_3 uptake in STS droplets at higher temperatures under the enhanced aerosol loading from Mt. Pinatubo (Santee *et al.*, 1998). Both of these findings are in good agreement with the equilibrium STS model calculations of Carslaw *et al.* (1994).

3.5 OUTSTANDING ISSUES IN STRATOSPHERIC PARTICLES

One outstanding issue that must be resolved is the quantification of the non-volcanic background SSA level, which cannot be determined from the current data record because of the influence of volcanoes. Understanding of this background level is required to assess the validity of models of SSA production, to allow detection of possible future anthropogenic trends, and to determine the partitioning of ozone destruction amongst the chlorine, hydrogen, and nitrogen radical families (Wennberg *et al.*, 1994). Except for this issue, there is a general consistency of SSA observations with dynamical and microphysical modeling results.

In contrast, the interpretation of PSC observations still suffers from many unknowns and uncertainties with relevance to stratospheric chemistry (see Chapter 7). Recent progress in understanding PSCs came with the recognition that some of these clouds are liquid and do not require any kind of phase transition during their growth. While there is overwhelming evidence for the existence of solid particles in the stratosphere, our understanding of the mechanisms of phase transitions leading to the formation of solid PSC particles is still very poor. Solid particle formation could be crucial for the heterogeneous chemical reactions occurring on PSCs because the solid HNO_3 hydrates can exist under warmer conditions than STS clouds. Furthermore, solidification of a few particles by some highly selective mechanism appears to be a necessary prerequisite for the denitrification of the polar vortices, which may lead to enhanced polar ozone destruction. For the modeling of Type 1a PSC formation, knowledge of the particle size distribution and phase at one particular point in time may not be sufficient, but rather the full thermal history of the air parcel containing the cloud particles may be required. There is a need for quasi-Lagrangian in situ measurements to follow particle evolution and to observe freezing events themselves.

Another outstanding issue is the effect that increases in source gases coupled with decreasing stratospheric temperatures may have on stratospheric particles. There are reports of an upward trend in H_2O, and Chapter 5 presents clear evidence of a long-term cooling in the lower stratosphere. An increase in HNO_3 in the lower stratosphere might also be expected because there is an upward trend in tropospheric N_2O. Both the surface area and heterogeneous reactivity of SSA should increase under these conditions. Surface area increases should be small, but there may be larger increases in heterogeneous reactivity (see Chapter 7).

More significant changes may occur in the properties and heterogeneous reactivity of Type 1b PSCs. For example, Figure 3-1 illustrates that particle surface area increases by 5-18% per 0.1 K temperature decrease in the interval between 192 and 191 K, around the STS threshold temperature. This could be of particular significance in the Arctic, where PSCs often form in limited synoptic-scale cold-temperature areas. The STS threshold temperature is also shifted upward by approximately 1 K per 1 ppm increase in H_2O in the lower strato-

sphere. An example of this sensitivity is shown by HALOE data late in the 1993 Antarctic spring, where there was enhanced PSC development due to an intrusion of H_2O from lower latitudes (Hervig *et al.*, 1997). However, no trend in PSCs is discernible in the present satellite PSC data record because of the relatively short record length and the large interannual variability in the number of clouds observed.

It also should be noted that current models used for assessment calculations are limited in the accuracy to which they can represent PSC processes. For example, only large-scale PSC events can be reproduced in global models because of the models' relatively coarse resolution. Furthermore, most models include relatively simple microphysical assumptions or parameterizations, whereas field observations show that PSCs exhibit very complex and variable behavior. 2-D models inherently cannot represent the fact that PSC formation is not zonally symmetric, particularly in the Arctic, as shown by SAM II and POAM II data. Some progress has been made in this area (Considine *et al.*, 1994), whereby PSC formation is modeled using statistical temperature fluctuations about the zonal mean values, hence producing more PSCs than would occur using zonal average temperatures. Even a 3-D formulation has limitations in capturing small-scale phenomena such as gravity or mountain waves, where rapid temperature fluctuations may result in nonequilibrium microphysical processes that could be important in forming solid PSC particles, especially in the Arctic. The integral role of such phenomena in ozone depletion is unclear.

REFERENCES

Abbas, M.M., H.A. Michelsen, M.R. Gunson, M.C. Abrams, M.J. Newchurch, R.J. Salawitch, A.Y. Chang, A. Goldman, F.W. Irion, G.L. Manney, E.J. Moyer, R. Nagaraju, C.P. Rinsland, G.P. Stiller, and R. Zander, Seasonal-variations of water-vapor in the lower stratosphere inferred from ATMOS/ATLAS-3 measurements of H_2O and CH_4, *Geophys. Res. Lett.*, *23*, 2401-2404, 1996.

Adriani, A., T. Deshler, G.P. Gobbi, B.J. Johnson, and G. Di Donfrancesco, Polar stratospheric clouds over McMurdo, Antarctica, during the spring 1991: Lidar and particle counter measurements, *Geophys. Res. Lett.*, *19*, 1755-1758, 1992.

Adriani, A., T. Deshler, G. Di Donfrancesco, and G.P. Gobbi, Polar stratospheric clouds and volcanic aerosol during spring 1992 over McMurdo Station, Antarctica: Lidar and particle counter comparisons, *J. Geophys. Res.*, *100*, 25877-25897, 1995.

Anderson, J., and V.K. Saxena, Temporal changes of Mount Pinatubo aerosol characteristics over northern midlatitudes derived from SAGE II extinction measurements, *J. Geophys. Res.*, *101*, 19455-19463, 1996.

Ångström, A., On the atmospheric transmission of sun radiation and on dust in the air, *Geogr. Ann.*, *11*, 156-166, 1908.

Anthony, S.E., R.T. Tisdale, R.S. Disselkamp, M.A. Tolbert, and J.C. Wilson, FTIR studies of low-temperature sulfuric-acid aerosols, *Geophys. Res. Lett.*, *22*, 1105-1108, 1995.

Arnold, F., J. Curtius, S. Spreng, and T. Deshler, Stratospheric aerosol sulfuric acid: First direct in situ measurements using a novel balloon-based mass spectrometer apparatus, *J. Atmos. Chem.*, *30*, 3-10, 1998.

Ayers, G.P., R.W. Gillett, and J.L. Gras, On the vapor pressure of sulfuric acid, *Geophys. Res. Lett.*, *7*, 433-436, 1980.

Barnes, J.E., and D.J. Hofmann, Lidar measurements of stratospheric aerosol over Mauna Loa Observatory, *Geophys. Res. Lett.*, *24*, 1923-1926, 1997.

Baumgardner, D., J.E. Dye, B.W. Gandrud, and R.G. Knollenberg, Interpretation of measurements made by the forward scattering spectrometer probe (FSSP-300) during the airborne Arctic stratospheric expedition, *J. Geophys. Res.*, *97*, 8035-8046, 1992.

Baumgardner, D., J.E. Dye, B. Gandrud, K. Barr, K. Kelly, and K.R. Chan, Refractive indices of aerosols in the upper troposphere and lower stratosphere, *Geophys. Res. Lett.*, *23*, 749-752, 1996.

Bekki, S., On the possible role of aircraft-generated soot in middle latitude ozone depletion, *J. Geophys. Res.*, *100*, 7195-7202, 1995.

Bekki, S., and J.A. Pyle, Two-dimensional assessment of the impact of aircraft sulphur emissions on the stratospheric sulphate aerosol layer, *J. Geophys. Res.*, *97*, 15839-15847, 1992.

Bekki, S., M.P. Chipperfield, J.A. Pyle, J.J. Remedios, S.E. Smith, R.G. Grainger, A. Lambert, J.B. Kumer, and J.L. Mergenthaler, Coupled aerosol-chemical modeling of UARS HNO_3 and N_2O_5 measurements in the arctic upper stratosphere, *J. Geophys. Res.*, *102*, 8977-8984, 1997.

Beyer, K.D., S.W. Seago, H.Y. Chang, and M.J. Molina, Composition and freezing of aqueous H_2SO_4/ HNO_3 solutions under polar stratospheric conditions, *Geophys. Res. Lett.*, *21*, 871-874, 1994.

Beyerle, G., R. Neuber, O. Schrems, F. Wittrock, and B. Knudsen, Multiwavelength lidar measurements of stratospheric aerosols above Spitsbergen during winter 1992/93, *Geophys. Res. Lett.*, *21*, 57-60, 1994.

Beyerle, G., B. Luo, R. Neuber, T. Peter, and I.S. McDermid, Temperature dependence of ternary solution particle volumes as observed by lidar in the Arctic stratosphere during 1992/93, *J. Geophys. Res.*, *102*, 3603-3609, 1997.

Biermann, U.M., T. Presper, T. Koop, J. Mößinger, P.J. Crutzen, and T. Peter, The unsuitability of meteoritic and other nuclei for polar stratospheric cloud freezing, *Geophys. Res. Lett.*, *23*, 1693-1696, 1996.

Bigg, E.K., Stratospheric particles, *J. Atmos. Sci.*, *32*, 910-917, 1975.

Blake, D.F., and K. Kato, Latitudinal distribution of black carbon soot in the upper troposphere and lower stratosphere, *J. Geophys. Res.*, *100*, 7195-7202, 1995.

Borrmann, S., J.E. Dye, D. Baumgardner, M.H. Proffitt, J.J. Margitan, J.C. Wilson, H.H. Jonsson, C.A. Brock, M. Loewenstein, J.R. Podolske, and G.V. Ferry, Aerosols as dynamical tracers in the lower stratosphere: Ozone versus aerosol correlation after the Mount Pinatubo eruption, *J. Geophys. Res.*, *100*, 11147-11156, 1995.

Borrmann, S., S. Solomon, J.E. Dye, and B. Luo, The potential of cirrus clouds for heterogeneous chlorine activation, *Geophys. Res. Lett.*, *23*, 2133-2136, 1996.

Borrmann, S., S. Solomon, L. Avallone, D. Toohey, and D. Baumgardner, On the occurrence of ClO in cirrus clouds and volcanic aerosol in the tropopause region, *Geophys. Res. Lett.*, *24*, 2011-2014, 1997a.

Borrmann, S., S. Solomon, J.E. Dye, D. Baumgardner, K.K. Kelly, and K.R. Chan, Heterogeneous reactions on stratospheric background aerosols, volcanic sulfuric acid droplets, and type I polar stratospheric clouds: Effects of temperature fluctuations and differences in particle phase, *J. Geophys. Res.*, *102*, 3639-3648, 1997b.

Brock, C.A., P. Hamill, J.C. Wilson, H.H. Jonsson, and K.R. Chan, Particle formation in the upper tropical troposphere: A source of nuclei for the stratospheric aerosol, *Science*, *270*, 1650-1653, 1995.

Browell, E.V., C.F. Butler, S. Ismail, P.A. Robinette, A.F. Carter, N.S. Higdon, O.B. Toon, M.R. Schoeberl, and A.F. Tuck, Airborne lidar observations in the wintertime Arctic stratosphere: Polar stratospheric clouds, *Geophys. Res. Lett.*, *17*, 385-388, 1990.

Capps, C.D., R.L. Henning, and G.M. Hess, Analytic inversion of remote sensing data, *Appl. Opt.*, *21*, 3581-3587, 1982.

Carslaw, K.S., B.P. Luo, S.L. Clegg, T. Peter, P. Brimblecombe, and P.J. Crutzen, Stratospheric aerosol growth and HNO_3 gas phase depletion from coupled HNO_3 and water uptake by liquid particles, *Geophys. Res. Lett.*, *21*, 2479-2482, 1994.

Carslaw, K.S., S.L. Clegg, and P. Brimblecombe, A thermodynamic model of the system HCl-HNO_3-H_2SO_4-H_2O including solubilities of HBr, from <200 K to 328 K, *J. Phys. Chem.*, *99*, 11557-11574, 1995.

Carslaw, K.S., T. Peter, and S.L. Clegg, Modeling the composition of liquid stratospheric aerosols, *Rev. Geophys.*, *35*, 125-154, 1997.

Carslaw, K.S., M. Wirth, A. Tsias, B.P. Luo, A. Dörnbrack, M. Leutbecher, H. Volkert, W. Renger, J.T. Bacmeister, and T. Peter, Particle processes and chemistry in remotely observed mountain polar stratospheric clouds, *J. Geophys. Res.*, *103*, 5785-5796, 1998.

Chazette, P., C. David, J. Lefrere, S. Godin, J. Pelon, and G. Mégie, Comparative lidar study of the optical, geometrical, and dynamical properties of stratospheric post-volcanic aerosols, following the eruptions of El Chichón and Mount Pinatubo, *J. Geophys. Res.*, *101*, 23195-23207, 1995.

Chin, M., and D.D. Davis, Global sources and sinks of OCS and CS_2 and their distributions, *Global Biogeochem. Cycles*, *7*, 321-337, 1993.

Chin, M., and D.D. Davis, A reanalysis of carbonyl sulfide as a source of stratospheric background sulfur aerosol, *J. Geophys. Res.*, *100*, 8993-9005, 1995.

Considine, D.B., A.R. Douglass, and C.H. Jackman, Effects of a polar stratospheric cloud parameterization on ozone depletion due to stratospheric aircraft in a two-dimensional model, *J. Geophys. Res.*, *99*, 18879-18894, 1994.

Crutzen, P.J., The possible importance of CSO for the sulfate layer of the stratosphere, *Geophys. Res. Lett.*, *3*, 73-76, 1976.

David, C., S. Godin, G. Mégie, Y. Emery, and C. Flesia, Physical state and composition of polar stratospheric clouds inferred from airborne lidar measurements during SESAME, *J. Atmos. Chem.*, *27*, 1-16, 1997.

David, C., S. Bekki, S. Godin, G. Mégie, and M.P. Chipperfield, Polar stratospheric clouds climatology over Dumont d'Urville between 1989 and 1993 and the influence of volcanic aerosols on their formation, *J. Geophys. Res.*, *103*, 22163-22180, 1998.

Del Guasta, M., M. Morandi, L. Stefanutti, B. Stein, and J.P. Wolf, Derivation of Mount Pinatubo stratospheric aerosol mean size distribution by means of a multiwavelength lidar, *Appl. Opt.*, *33*, 5690-5697, 1994.

Del Negro, L.A., D.W· Fahey, S.G. Donnelly, R.S. Gao, E.R. Keim, R.C. Wamsley, E.L. Woodbridge, J.E. Dye, D. Baumgardner, B.W. Gandrud, J.C. Wilson, H.H. Jonsson, M. Loewenstein, J.R. Podolske, C.R. Webster, R.D. May, D.R. Worsnop, A. Tabazadeh, M.A. Tolbert, K.K. Kelly, and K.R. Chan, Evaluating the role of NAT, NAD, and liquid $H_2SO_4/H_2O/HNO_3$ solutions in Antarctic polar stratospheric cloud aerosol: Observations and implications, *J. Geophys. Res.*, *102*, 13255-13282, 1997.

Deshler, T., and S.J. Oltmans, Vertical profiles of volcanic aerosol and polar stratospheric clouds above Kiruna, Sweden: Winters 1993 and 1995, *J. Atmos. Chem.*, *30*, 11-23, 1998.

Deshler, T., A. Adriani, D.J. Hofmann, and G.P. Gobbi, Evidence for denitrification in the 1990 Antarctic spring stratosphere: II, Lidar and aerosol measurements, *Geophys. Res. Lett.*, *18*, 1999-2002, 1991.

Deshler, T., D.J. Hofmann, B.J. Johnson, and W.R. Rozier, Balloon-borne measurements of Pinatubo aerosol size distribution and volatility at Laramie, Wyoming during the summer of 1991, *Geophys. Res. Lett.*, *19*, 199-202, 1992.

Deshler, T., B.J. Johnson, and W.R. Rozier, Balloonborne measurements of Pinatubo aerosol during 1991 and 1992 at 41°N, vertical profiles, size distribution, and volatility, *Geophys. Res. Lett.*, *20*, 1435-1438, 1993.

Deshler, T., B.J. Johnson, and W.R. Rozier, Changes in the character of polar stratospheric clouds over Antarctica in 1992 due to the Pinatubo volcanic aerosol, *Geophys. Res. Lett.*, *21*, 273-276, 1994a.

Deshler, T., T. Peter, R. Müller, and P.J. Crutzen, The lifetime of leewave-induced ice particles in the Arctic stratosphere: I, Balloonborne observations, *Geophys. Res. Lett.*, *21*, 1327-1330, 1994b.

Deshler, T., G.B. Liley, G. Bodeker, W.A. Matthews, and D.J. Hofmann, Stratospheric aerosol following Pinatubo: Comparison of the north and south midlatitudes using in situ measurements, *Adv. Space Res.*, *20*, 2057-2061, 1997.

Dessler, A.E., E.M. Weinstock, E.J. Hintsa, J.G. Anderson, C.R. Webster, R.D. May, J.W. Elkins, and G.S. Dutton, An examination of the total hydrogen budget of the lower stratosphere, *Geophys. Res. Lett.*, *21*, 2563-2566, 1994.

Drdla, K., A. Tabazadeh, R.P. Turco, M.Z. Jacobson, J.E. Dye, C. Twohy, and D. Baumgardner, Analysis of the physical state of one Arctic polar stratospheric cloud based on observations, *Geophys. Res. Lett.*, *21*, 2475-2478, 1994.

Dye, J.E., B.W. Gandrud, D. Baumgardner, and L. Sanford, A survey of particle measurements in the Arctic from the forward scattering spectrometer probe model 300, *Geophys. Res. Lett.*, *17*, 409-412, 1990a.

Dye, J.E., B.W. Gandrud, D. Baumgardner, K.R. Chan, G.V. Ferry, M. Loewenstein, K.K. Kelly, and J.C. Wilson, Observed particle evolution in the polar stratospheric cloud of January 24, 1989, *Geophys. Res. Lett.*, *17*, 413-416, 1990b.

Dye, J.E., D. Baumgardner, B.W. Gandrud, S.R. Kawa, K.K. Kelly, M. Loewenstein, G.V. Ferry, K.R. Chan, and B.L. Gary, Particle size distribution in Arctic polar stratospheric clouds, growth and freezing of sulfuric acid droplets, and implications for cloud formation, *J. Geophys. Res.*, *97*, 8015-8034, 1992.

Dye, J.E., D. Baumgardner, B.W. Gandrud, K. Drdla, K. Barr, D.W· Fahey, L.A. Del Negro, A. Tabazadeh, H.H. Jonsson, J.C. Wilson, M. Loewenstein, J.R. Podolske, and K.R. Chan, In-situ observations of an Antarctic polar stratospheric cloud: Similarities with Arctic observations, *Geophys. Res. Lett*., *23*, 1913-1916, 1996.

Engel, A., C. Schiller, U. Schmidt, R. Borchers, H. Ovarlez, and J. Ovarlez, The total hydrogen budget in the arctic winter stratosphere during the European Arctic Stratospheric Ozone Experiment, *J. Geophys. Res.*, *101*, 14495-14503, 1996.

Fabian, P., W.F. Libby, and C.E. Palmer, Stratospheric residence time and interhemispheric mixing of strontium 90 from fallout in rain, *J. Geophys. Res.*, *73*, 3611-3616, 1968.

Fahey, D.W·, K.K. Kelly, G.V. Ferry, L.R. Poole, J.C. Wilson, D.M. Murphy, M. Loewenstein, and K.R. Chan, In situ measurements of total reactive nitrogen, total water, and aerosol in a polar stratospheric cloud in the Antarctic, *J. Geophys. Res*., *94*, 11299-11315, 1989.

Fahey, D.W·, E.R. Keim, K.A. Boering, C.A. Brock, J.C. Wilson, S. Anthony, T.F. Hanisco, P.O. Wennberg, R.C. Miake-Lye, R.J. Salawitch, N. Louisnard, E.L. Woodbridge, R.S. Gao, S.G. Donnelly, R.C. Wamsley, L.A. Del Negro, B.C. Daube, S.C. Wofsy, C.R. Webster, R.D. May, K.K. Kelly, M. Loewenstein, J.R. Podolske, and K.R. Chan, Emission measurements of the Concorde supersonic aircraft in the lower stratosphere, *Science*, *270*, 70-74, 1995.

Fairlie, T.D., Three-dimensional transport simulations of the dispersal of volcanic aerosol from Mount Pinatubo, *Quart. J. Roy. Meteorol. Soc.*, *121*, 1943-1980, 1995.

Farlow, N.H., G.V. Ferry, H.Y. Lem, and D.M. Haynes, Latitudinal variations of stratospheric aerosols, *J. Geophys. Res.*, *84*, 733-743, 1979.

Ferry, G.V., E. Neish, M. Schultz, and R.F. Pueschel, Concentrations and size distributions of Antarctic stratospheric aerosols, *J. Geophys Res*., *94*, 16459-16474, 1989.

Fiocco, G., and G. Grams, Observation of aerosol layer of 20 km by optical radar, *J. Atmos. Sci.*, *21*, 323-324, 1964.

Flesia, C., A. Mugnai, Y. Emery, S. Godin, L. de Schoulepnikoff, and V. Mitev, Interpretation of lidar depolarization measurements of the Pinatubo stratospheric aerosol layer during EASOE, *Geophys. Res. Lett.*, *21*, 1443-1446, 1994.

Fromm, M.D., R.M. Bevilacqua, E.P. Shettle, J. Hornstein, J.D. Lumpe, S.T. Massie, and K.H. Fricke, Observations of Antarctic polar stratospheric clouds by POAM II: 1994-1996, *J. Geophys. Res*., *102*, 23659-23672, 1997.

Gable, C.M., H.F. Betz, and S.H. Maron, Phase equilibria of the system sulfur trioxide-water, *J. Amer. Chem. Soc*., *72*, 1445-1448, 1950.

Gandrud, B.W·, J.E. Dye, D. Baumgardner, G.V. Ferry, M. Loewenstein, K.R. Chan, B. Gary, and K.K. Kelly, The January 30, 1989 Arctic polar stratospheric cloud (PSC) event: Evidence for a mechanism of dehydration, *Geophys. Res. Lett*., *17*, 457-459, 1990.

Glaccum, W., R.L. Lucke, R.M. Bevilacqua, E.P. Shettle, J.S. Hornstein, D.T. Chen, J.D. Lumpe, S.S. Krigman, D.J. Debrestian, M.D. Fromm, F. Dalaudier, E. Chassefière, C. Deniel, C.E. Randall, D.W. Rusch, J.J. Olivero, C. Brogniez, J. Lenoble, and R. Kremer, The Polar Ozone and Aerosol Measurement (POAM II) instrument, *J. Geophys. Res*., *101*, 14479-14787, 1996.

Gobbi, G.P., Lidar estimation of stratospheric aerosol properties: Surface, volume, and extinction to backscatter ratio, *J. Geophys. Res*., *100*, 11219-11235, 1995.

Gobbi, G.P., and A. Adriani, Mechanisms of formation of stratospheric clouds observed during the Antarctic late winter of 1992, *Geophys. Res. Lett.*, *20*, 1427-1430, 1993.

Godin, S., G. Mégie, C. David, D. Haner, C. Flesia, and Y. Emery, Airborne lidar observation of mountain-wave-induced polar stratospheric clouds during EASOE, *Geophys. Res. Lett.*, *21*, 1335-1338, 1994.

Godin, S., C. David, and M. Guirlet, Evolution of the Mt. Pinatubo volcanic cloud and analysis of its effect on the ozone amount as observed from ground-based measurements performed in northern and southern latitudes, in *The Mount Pinatubo Eruption: Effects on the Atmosphere and Climate*, NATO ASI Series, Series I Global Environmental Change, Vol. 42, edited by G. Fiocco, D. Fua, and G. Visconti, Springer-Verlag, Berlin, 1996.

Goodman, J., O.B. Toon, R.F. Pueschel, K.G. Snetsinger, and S. Verma, Antarctic stratospheric ice crystals, *J. Geophys. Res.*, *94*, 16449-16457, 1989.

Goodman, J., K.G. Snetsinger, R.F. Pueschel, and S. Verma, Decay of Mount Pinatubo volcanic perturbation, *Geophys. Res. Lett.*, *21*, 1129-1132, 1994.

Goodman, J., S. Verma, R.F. Pueschel, P. Hamill, G.V. Ferry, and D. Webster, New evidence of size and composition of polar stratospheric cloud particles, *Geophys. Res. Lett.*, *24*, 615-618, 1997.

Grainger, R.G., A. Lambert, C.D. Rodgers, F.W. Taylor, and T. Deshler, Stratospheric aerosol effective radius, surface area, and volume estimated from infrared measurements, *J. Geophys. Res.*, *100*, 16507-16518, 1995.

Grant, W.B., E.V. Browell, C.S. Long, L.L. Stowe, R.G. Grainger, and A. Lambert, Use of volcanic aerosols to study the tropical stratospheric reservoir, *J. Geophys. Res.*, *101*, 3973-3988, 1996.

Griggs, M., Satellite measurements of tropospheric aerosols, *Adv. Space Res.*, *2*, 109-118, 1983.

Gruner, P., and H. Kleinert, Die dammerungerscheinen, *Probl. Kosm. Phys.*, *10*, 1-113, 1927.

Hammer, C.U., H.B. Clausen, and W. Dansgaard, Greenland ice sheet evidence of postglacial volcanism and its climatic impact, *Nature*, *288*, 230-235, 1980.

Hanson, D.R., and K. Mauersberger, Laboratory studies of the nitric acid trihydrate: Implication for the south polar stratosphere, *Geophys. Res. Lett.*, *15*, 855-858, 1988.

Hanson, D.R., A.R. Ravishankara, and S. Solomon, Heterogeneous reactions in sulfuric acid aerosols: A framework for model calculations, *J. Geophys. Res.*, *99*, 3615-3629, 1994.

Harries, J.E., J.M. Russell III, A.F. Tuck, L.L. Gordley, P. Purcell, K. Stone, R.M. Bevilacqua, M. Gunson, G. Nedoluha, and W.A. Traub, Validation of measurements of water vapor from the Halogen Occultation Experiment (HALOE), *J. Geophys. Res.*, *101*, 10205-10216, 1996.

Herber, A., L.W. Thomason, V.F. Radinov, and U. Leiter, Comparison of trends in the tropospheric and stratospheric aerosol optical depths in the Antarctic, *J. Geophys. Res.*, *98*, 18441-18447, 1993.

Hervig, M.E., J.M. Russell III, L.L. Gordley, J.H. Park, S.R. Drayson, and T. Deshler, Validation of aerosol measurements from the Halogen Occulation Experiment, *J. Geophys. Res.*, *101*, 10267-10275, 1996.

Hervig, M.E., K.S. Carslaw, T. Peter, T. Deshler, L.L. Gordley, G. Redaelli, U. Biermann, and J.M. Russell III, Polar stratospheric clouds due to vapor enhancement: HALOE observations of the Antarctic vortex in 1993, *J. Geophys. Res.*, *102*, 28185-28193, 1997.

Hervig, M.E., T. Deshler, and J.M. Russell III, Aerosol size distributions obtained from HALOE spectral extinction measurements, *J. Geophys. Res.*, *103*, 1573-1583, 1998.

Hitchman, M.H., M. McKay, and C.R. Trepte, A climatology of stratospheric aerosol, *J. Geophys. Res.*, *99*, 20689-20700, 1994.

Hofmann, D.J., Increase in the stratospheric background sulfuric acid aerosol mass in the past 10 years, *Science*, *248*, 996-1000, 1990a.

Hofmann, D.J., Measurement of the condensation nuclei profile to 31 km in the Arctic in January 1989 and comparisons with Antarctic measurements, *Geophys. Res. Lett.*, *17*, 357-360, 1990b.

Hofmann, D.J., Stratospheric cloud micro-layers and small-scale temperature variations in the Arctic in 1989, *Geophys. Res. Lett.*, *17*, 369-372, 1990c.

Hofmann, D.J., Aircraft sulphur emissions, *Nature*, *349*, 659, 1991.

Hofmann, D.J., and T. Deshler, Comparison of stratospheric clouds in the Antarctic and the Arctic, *Geophys. Res. Lett.*, *16*, 1429-1432, 1989.

Hofmann, D.J., and T. Deshler, Balloonborne measurements of polar stratospheric clouds and ozone at -93˚C in the Arctic in February 1990, *Geophys. Res. Lett.*, *17*, 2185-2188, 1990.

Hofmann, D.J., and T. Deshler, Stratospheric cloud observations during formation of the Antarctic ozone hole in 1989, *J. Geophys. Res.*, *96*, 2897-2912, 1991.

Hofmann, D.J., and J.M. Rosen, Balloon observations of a particle layer injected by a stratospheric aircraft at 23 km, *Geophys. Res. Lett.*, *5*, 511-514, 1978.

Hofmann, D.J., and J.M. Rosen, Balloon-borne observations of stratospheric aerosol and condensation nuclei during the year following the Mt. St. Helens eruption, *J. Geophys. Res.*, *87*, 11039-11061, 1982.

Hofmann, D.J., and J.M. Rosen, Stratospheric sulfuric acid fraction and mass estimate for the 1982 volcanic eruption of El Chichón, *Geophys. Res. Lett.*, *4*, 313-316, 1983.

Hofmann, D.J., J.M. Rosen, T.J. Pepin, and R.G. Pinnick, Stratospheric aerosol measurements: I, Time variations at northern midlatitudes, *J. Atmos. Sci.*, *32*, 1446-1456, 1975.

Hofmann, D.J., J.M. Rosen, and W. Gringel, Delayed production of sulfuric acid condensation nuclei in the polar stratosphere from El Chichón volcanic vapors, *J. Geophys. Res.*, *90*, 2341-2354, 1985.

Hofmann, D.J., J.M. Rosen, and J.W. Harder, Aerosol measurements in the winter/spring Antarctic stratosphere: 1, Correlative measurements with ozone, *J. Geophys. Res.*, *93*, 665-676, 1988.

Hofmann, D.J., T. Deshler, F. Arnold, and H. Schlager, Balloon observations of nitric acid aerosol formation in the Arctic stratosphere: II, Aerosol, *Geophys. Res. Lett.*, *17*, 1279-1282, 1990.

Holton, J.R., P.H. Haynes, M.E. McIntyre, A.R. Douglass, R.B. Rood, and L. Pfister, Stratosphere-troposphere exchange, *Rev. Geophys.*, *33*, 403-439, 1995.

Höpfner, M., C.E. Blom, T. Blumenstock, H. Fischer, and T. Gulde, Evidence of the removal of gaseous HNO_3 inside the Arctic polar vortex in January 1992, *Geophys. Res. Lett.*, *22*, 149-152, 1996.

IPCC (Intergovernmental Panel on Climate Change), *Climate Change 1995*: *The Science of Climate Change*, edited by J.T Houghton, L.G. Meira Filho, J. Bruce, H. Lee, B.A. Callander, E. Haites, N.R.P. Harris, and K. Maskell, Cambridge University Press, Cambridge, U.K., 1996.

IPCC (Intergovernmental Panel on Climate Change), *Aviation and the Global Atmosphere: A Special Report of IPCC Working Groups I and III*, edited by J.T. Houghton, D. Lister, J. Penner, M. McFarland, D. Griggs, and D. Dokken, Cambridge University Press, Cambridge, U.K., 1999 (in preparation).

Iraci, L.T., A.M. Middlebrook, and M.A. Tolbert, Laboratory studies of the formation of polar stratospheric clouds: Nitric acid condensation on thin sulfuric acid films, *J. Geophys. Res.*, *100*, 20969-20977, 1995.

Iwasaka, Y., T. Hirasawa, and H. Fukunishi, Lidar measurements on the Antarctic stratospheric aerosol layer: I, Winter enhancement, *J. Geomagn. Geoelectr.*, *37*, 1087-1095, 1985.

Jackman, C.H., D.B. Considine, and E.L. Fleming, Space Shuttle's impact on the stratosphere: An update, *J. Geophys. Res.*, *101*, 12523-12529, 1996.

Jäger, H., Stratospheric aerosols: Observations, trends, and effects, *J. Aerosol Sci.*, *22*, suppl. 1, S517-S520, 1991.

Jäger, H., O. Uchino, T. Nagai, T. Fujimoto, V. Freudenthaler, and F. Homburg, Ground-based remote sensing of the decay of the Pinatubo eruption cloud at three Northern Hemisphere sites, *Geophys. Res. Lett.*, *23*, 607-610, 1996.

Jayaraman, A., S. Ramachandran, Y.B. Acharya, and B.H. Subbaraya, Pinatubo volcanic aerosol layer decay observed at Ahmedabad (23°N), India, using neodymium:yttrium/aluminum/garnet backscatter lidar, *J. Geophys. Res.*, *100*, 23209-23214, 1995.

Jones, A.E., S. Bekki, and J.A. Pyle, On the stratospheric impact of launching the Ariane 5 rocket, *J. Geophys. Res.*, *100*, 20969-20977, 1995.

Jonsson, H.H., J.C. Wilson, C.A. Brock, R.G. Knollenberg, R. Newton, J.E. Dye, D. Baumgardner, S. Borrmann, G.V. Ferry, R. Pueschel, D.C. Woods, and M.C. Pitts, Performance of a focused cavity aerosol spectrometer for measurements in the stratosphere of particle size in the 0.06-2.0 μm diameter range, *J. Atmos. Oceanic Technol.*, *12*, 115-129, 1995.

Jonsson, H.H., J.C. Wilson, C.A. Brock, J.E. Dye, G.V. Ferry, and K.R. Chan, Evolution of the stratospheric aerosol in the Northern Hemisphere following the June 1991 volcanic eruption of Mount Pinatubo: Role of tropospheric-stratospheric exchange and transport, *J. Geophys. Res.*, *101*, 1553-1570, 1996.

Junge, C.E., C.W. Changnon, and J.E. Manson, Stratospheric aerosols, *J. Meteorol.*, *18*, 81-108, 1961.

Kasibhatla, P.S., H. Levy, W.J. Moxim, and W.L. Chameides, The relative impact of stratospheric photochemical production on tropospheric NO_y levels: A model study, *J. Geophys. Res.*, *96*, 18631-18646, 1991.

Kent, G.S., and G.M. Hansen, Multiwavelength lidar observations of the decay phase of the stratospheric aerosol layer produced by the eruption of Mount Pinatubo in June 1991, *Appl. Opt.*, *37*, 3861-3872, 1998.

Khalil, M.A.K., and R.A. Rasmussen, Global sources, lifetimes and mass balances of carbonyl sulfide (OCS) and carbon-disulfide (CS_2) in the Earth's atmosphere, *Atmos. Environ.*, *18*, 1805-1813, 1984.

Koop, T., U.M. Biermann, W. Raber, B.P. Luo, P.J. Crutzen, and T. Peter, Do stratospheric aerosol droplets freeze above the ice frost point? *Geophys. Res. Lett.*, *22*, 917-920, 1995.

Koop, T., B.P. Luo, U.M. Biermann, P.J. Crutzen, and T. Peter, Freezing of $HNO_3/H_2SO_4/H_2O$ solutions at stratospheric temperatures: Nucleation statistics and experiments, *J. Phys. Chem. A*, *101*, 1117-1133, 1997.

Kotamarthi, V.R., M. Ko, D.K. Weisenstein, J.M. Rodriguez, and N.D. Sze, Effect of lightning on the concentration of odd nitrogen species in the lower stratosphere: An update, *J. Geophys. Res.*, *99*, 8167-8173, 1994.

Lambert, A., R.G. Grainger, C.D. Rodgers, F.W. Taylor, J.L. Mergenthaler, J.B. Kumer, and S.T. Massie, Global evolution of the Mt. Pinatubo volcanic aerosols observed by the infrared limb-sounding instruments CLAES and ISAMS on the Upper Atmospheric Research Satellite, *J. Geophys. Res.*, *102*, 1495-1512, 1997.

Langner, J., and H. Rodhe, A global three-dimensional model of the tropospheric sulfur cycle, *J. Atmos. Chem.*, *13*, 225-263, 1991.

Larsen, N., J.M. Rosen, N.T. Kjome, and B. Knudsen, Deliquescence and freezing of stratospheric aerosol observed by balloonborne backscattersondes, *Geophys. Res. Lett.*, *22*, 1233-1236, 1995.

Larsen, N., B.M. Knudsen, J.M. Rosen, N.T. Kjome, and E. Kyrö, Balloonborne backscatter observations of type 1 PSC formation: Inference about physical state from trajectory analysis, *Geophys. Res. Lett.*, *23*, 1091-1094, 1996.

Larsen, N., B.M. Knudsen, J.M. Rosen, N.T. Kjome, R. Neuber, and E. Kyrö, Temperature histories in liquid and solid polar stratospheric cloud formation, *J. Geophys. Res.*, *102*, 23505-23517, 1997.

Luo, B.P., T. Peter, and P.J. Crutzen, Freezing of stratospheric aerosol droplets, *Geophys. Res. Lett.*, *21*, 1447-1450, 1994.

Luo, B.P., K.S. Carslaw, T. Peter, and S.L. Clegg, Vapor-pressures of $H_2SO_4/HNO_3/HCl/HBr/H_2O$ solutions to low stratospheric temperatures, *Geophys. Res. Lett.*, *22*, 247-250, 1995.

Luo, B., U.K. Krieger, and T. Peter, Densities and refractive indices of $H_2SO_4/HNO_3/H_2O$ solutions to stratospheric temperatures, *Geophys. Res. Lett.*, *23*, 3707-3710, 1996.

MacKenzie, A.R., M. Kulmala, A. Laaksonen, and T. Vesala, On the theories of Type I polar stratospheric cloud formation, *J. Geophys. Res.*, *100*, 11275-11288, 1995.

Massie, S.T., J.C. Gille, D.P. Edwards, P.L. Bailey, L.V. Lyjak, C.A. Craig, C.P. Cavanaugh, J.L. Mergenthaler, A.E. Roche, J.B. Kumer, A. Lambert, R.G. Grainger, C.D. Rodgers, F.W. Taylor, J.M. Russell III, J.H. Park, T. Deshler, M.E. Hervig, E.F. Fishbein, J.W. Waters, and W.A. Lahoz, Validation studies using multiwavelength Cryogenic Limb Array Etalon Spectrometer (CLAES) observations of stratospheric aerosol, *J. Geophys. Res.*, *101*, 9757-9773, 1996.

Massie, S.T., J.E. Dye, D. Baumgardner, W.J. Randel, F. Wu, X. Tie, L. Pan, F. Figarol, G.P. Brasseur, M.L. Santee, W.G. Read, R.G. Grainger, A. Lambert, J.L. Mergenthaler, and A. Tabazadeh, Simultaneous observations of polar stratospheric clouds and HNO_3 over Scandinavia in January 1992, *Geophys. Res. Lett.*, *24*, 595-598, 1997.

McCormick, M.P., P. Hamill, T.J. Pepin, W.P. Chu, T.J. Swissler, and L.R. McMaster, Satellite studies of the stratospheric aerosol, *Bull. Amer. Meteorol. Soc.*, *60*, 1038-1046, 1979.

McCormick, M.P., H.M. Steele, P. Hamill, W.P. Chu, and T.J. Swissler, Polar stratospheric cloud sightings by SAM II, *J. Atmos. Sci.*, *39*, 1387-1397, 1982.

McCormick, M.P., G.S. Kent, W.H. Hunt, M.T. Osborn, L.R. Poole, and M.C. Pitts, Arctic polar stratospheric cloud observations by airborne lidar, *Geophys. Res. Lett.*, *17*, 381-384, 1990.

Meilinger, S.K., T. Koop, B.P. Luo, T. Huthwelker, K.S. Carslaw, U. Krieger, P.J. Crutzen, and T. Peter, Size-dependent stratospheric droplet composition in leewave temperature fluctuations and their potential role in PSC freezing, *Geophys. Res. Lett.*, *22*, 3031-3034, 1995.

Menzies, R.T., and D.M. Tratt, Evidence of seasonally dependent stratosphere troposphere exchange and purging of lower stratospheric aerosol from a multiyear lidar data set, *J. Geophys. Res.*, *100*, 3139-3148, 1995.

Mergenthaler, J.L., J.B. Kumer, and A.E. Roche, Distribution of Antarctic polar stratospheric clouds as seen by the CLAES experiment, *J. Geophys. Res.*, *102*, 19161-19170, 1997.

Middlebrook, A.M., L.T. Iraci, L.S. McNeill, B.G. Koehler, M.A. Wilson, O.W. Saastad, M.A. Tolbert, and D.R. Hanson, Fourier transform infrared studies of thin H_2SO_4/H_2O films: Formation, water uptake, and solid-liquid phase changes, *J. Geophys. Res.*, *98*, 20473-20481, 1993.

Mischenko, M.I., and K. Sassen, Depolarization of lidar returns by small ice crystals: An application to contrails, *Geophys. Res. Lett.*, *25*, 309-312, 1998.

Molina, M.J., R. Zhang, P.J. Wooldridge, J.R. McMahon, J.E. Kim, H.Y. Chang, and K. Beyer, Physical chemistry of the $H_2SO_4/HNO_3/H_2O$ system: Implications for polar stratospheric clouds, *Science*, *251*, 1418-1423, 1993.

Mote, P.W., K.H. Rosenlof, J.R. Holton, R.S. Harwood, and J.W. Waters, Seasonal-variations of water vapor in the tropical lower stratosphere, *Geophys. Res. Lett.*, *22*, 1093-1096, 1995.

Mote, P.W., K.H. Rosenlof, M.E. McIntyre, E.S. Carr, J.C. Gille, J.R. Holton, J.S. Kinnersley, H.C. Pumphrey, J.M. Russell III, and J.W. Waters, An atmospheric tape-recorder: The imprint of tropical tropopause temperatures on stratospheric water vapor, *J. Geophys. Res.*, *101*, 3989-4006, 1996.

Müller, K.P., M. Langer, K. Romke, and K.H. Fricke, PSCs and aerosols above Andøya during SESAME winters 1993/94 and 1994/95, in *Polar Stratospheric Ozone 1995*, Air Pollution Research Report 56, edited by J.A. Pyle, N.R.P. Harris, and G.T. Amanatidis, pp. 122-125, European Commission, 1995.

Murphy, D.M., and B.L. Gary, Mesoscale temperature fluctuations and polar stratospheric clouds, *J. Atmos. Sci.*, *52*, 1753-1760, 1995.

Nagai, T., O. Uchino, T. Itabe, T. Shibata, K. Mizutani, and T. Fujimoto, Polar stratospheric clouds observed at Eureka (80N, 86W) in the Canadian Arctic during the 1994/1995 winter, *Geophys. Res. Lett.*, *24*, 2243-2246, 1997.

Nedoluha, G.E., R.M. Bevilacqua, R.M. Gomez, D.E. Siskind, B.C. Hicks, J.M. Russell III, and B.J. Connor, Increases in middle atmospheric water vapor observed by the Halogen Occultation Experiment and the ground-based Water Vapor Millimeter-wave Spectrometer from 1991-1997, *J. Geophys. Res.*, *103*, 3531-3543, 1998.

Oltmans, S.J., and D.J. Hofmann, Increase in lower stratospheric water vapor at a midlatitude Northern Hemisphere site from 1981 to 1994, *Nature*, *374*, 146-149, 1995.

Osborn, M.T., R.J. DeCoursey, C.R. Trepte, D.M. Winker, and D.C. Woods, Evolution of the Pinatubo volcanic cloud over Hampton, Virginia, *Geophys. Res. Lett.*, *22*, 1101-1104, 1995.

Pawson, S., B. Naujokat, and K. Labitzke, On the polar stratospheric cloud formation potential of the northern stratosphere, *J. Geophys. Res.*, *100*, 23215-23225, 1995.

Pepin, T.J., M.P. McCormick, W.P. Chu, F. Simon, T.J. Swissler, R.R. Adams, K.R. Crumbly, and W.H. Fuller, Jr., *Stratospheric Aerosol Measurements*, NASA SP-421, pp. 127-136, National Aeronautics and Space Administration, 1977.

Peter, T., Microphysics and heterogeneous chemistry of polar stratospheric clouds, *Ann. Rev. Phys. Chem.*, *48*, 779-816, 1997.

Pitari, G., V. Rizi, L. Ricciardulli, and G. Visconti, High-speed civil transport impact: Role of sulfate, nitric acid trihydrate, and ice aerosols studied with a 2-dimensional model including aerosol physics, *J. Geophys. Res.*, *98*, 23141-23164, 1993.

Pitts, M.C., L.R. Poole, and M.P. McCormick, SAGE II observations of polar stratospheric clouds near 50°N January 31-February 2, 1989, *Geophys. Res. Lett.*, *17*, 405-408, 1990.

Plumb, R.A., and R.C. Bell, A model of the quasi-biennial oscillation on an equatorial beta-plane, *Quart. J. Roy. Meteorol. Soc.*, *108*, 335-352, 1982.

Pollack, J.B., O.B. Toon, and E.F. Danielsen, The El Chichón volcanic cloud: An introduction, *Geophys. Res. Lett.*, *19*, 805-808, 1983.

Poole, L.R., and M.P. McCormick, Airborne lidar observations of Arctic polar stratospheric clouds: Indications of two distinct growth stages, *Geophys. Res. Lett.*, *15*, 21-23, 1988.

Poole, L.R., and M.C. Pitts, Polar stratospheric cloud climatology based on Stratospheric Aerosol Measurement II observations from 1978 to 1989, *J. Geophys. Res.*, *99*, 13083-13089, 1994.

Post, M.J., C.J. Grund, A.M. Weickmann, K.R. Healy, and R.J. Willis, Comparison of Mount Pinatubo and El Chichón volcanic events: Lidar observations at 10.6 and 0.69 μm, *J. Geophys. Res.*, *101*, 3929-3940, 1996.

Pueschel, R.F., Stratospheric aerosols: Formation, properties, effects, *J. Aerosol. Sci.*, *27*, 383-402, 1996.

Pueschel, R.F., K.G. Snetsinger, J.K. Goodman, O.B. Toon, G.V. Ferry, V.R. Overbeck, J.M. Livingtson, S. Verna, W. Fong, W.L. Starr, and R.K. Chan, Condensed nitrate, sulfate, and chloride in Antarctic stratospheric aerosols, *J. Geophys. Res.*, *94*, 11271-11284, 1989.

Pueschel, R.F., G.V. Ferry, K.G. Snetsinger, J. Goodman, J. Dye, D. Baumgardner, and B.W. Gandrud, A case of type I polar stratospheric cloud formation by heterogeneous nucleation, *J. Geophys. Res.*, *97*, 8105-8114, 1992.

Pyle, D.M., P.D. Beattie, and G.J.S. Bluth, Sulfur emissions to the stratosphere from explosive volcanic eruptions, *Bull. Volcanol.*, *57*, 663-671, 1996.

Ravishankara, A.R., and D.R. Hanson, Differences in the reactivity of type I polar stratospheric clouds depending on phase, *J. Geophys. Res.*, *101*, 3885-3890, 1996.

Remsberg, E.E., P.P. Bhatt, and J.M. Russell, Estimates of the water-vapor budget of the stratosphere from UARS HALOE data, *J. Geophys. Res.*, *101*, 6749-6766, 1996.

Rinsland, C.P., G.K. Yue, M.R. Gunson, R. Zander, and M.C. Abrams, Mid-infrared extinction by sulfate aerosols from the Mt. Pinatubo eruption, *J. Quant. Spectrosc. Radiat. Transfer*, *52*, 241-252, 1994.

Rinsland, C.P., M.R. Gunson, R.J. Salawitch, H.A. Michelsen, R. Zander, M.J. Newchurch, M.M. Abbas, M.C. Abrams, G.L. Manney, A.Y. Chang, F.W. Irion, A. Goldman, and E. Mahieu, Trends of OCS, HCN, SF_6, $CHClF_2$, (HCFC-22) in the lower stratosphere from 1985 and 1994 Atmospheric Trace Molecule Spectroscopy experiment measurements near 30˚N latitude, *Geophys. Res. Lett.*, *23*, 2349-2352, 1996.

Rosen, J.M., The vertical distribution of dust to 30 km, *J. Geophys. Res.*, *69*, 4673-4676, 1964.

Rosen, J.M., The boiling point of stratospheric aerosols, *J. Appl. Meteorol.*, *16*, 52-56, 1971.

Rosen, J.M., and D.J. Hofmann, Stratospheric condensation nuclei, *J. Appl. Meteorol.*, *16*, 56-62, 1977.

Rosen, J.M., and N.T. Kjome, Backscattersonde: A new instrument for atmospheric aerosol research, *J. Appl. Opt.*, *30*, 1552-1561, 1991.

Rosen, J.M., S.J. Oltmans, and W.E. Evans, Balloonborne observations of PSCs, frost point, ozone, and nitric acid in the north polar vortex, *Geophys. Res. Lett.*, *16*, 791-794, 1989.

Rosen, J.M, N.T. Kjome, and S.J. Oltmans, Observations of backscatter, particle concentration, and frost point in the north polar vortex stratospheric clouds, *Geophys. Res. Lett.*, *17*, 1271-1274, 1990.

Rosen, J.M., N.T. Kjome, and S.J. Oltmans, Simultaneous ozone and polar stratospheric cloud observations at South Pole Station during winter and spring 1991, *J. Geophys. Res.*, *98*, 12741-12751, 1993.

Rosen, J.M., N.T. Kjome, R.L. McKenzie, and J. B. Liley, Decay of Mount Pinatubo aerosol at midlatitudes in the Northern and Southern Hemispheres, *J. Geophys. Res.*, *99*, 25733-25739, 1994a.

Rosen, J.M., N.T. Kjome, H. Fast, and N. Larsen, Volcanic aerosol and polar stratospheric clouds in the winter 1992/93 north polar vortex, *Geophys. Res. Lett.*, *21*, 61-64, 1994b.

Rosen, J.M., N.T. Kjome, N. Larsen, B.M. Knudsen, E. Kyrö, R. Kivi, J. Karhu, R. Neuber, and I. Beninga, Polar stratospheric threshold temperatures, *J. Geophys. Res.*, *102*, 28195-28202, 1997.

Russell, P.B., J.M. Livingston, E.G. Dutton, R.F. Pueschel, J.A. Reagan, T.E. DeFoor, M.A. Box, D. Allen, P. Pilewskie, B.M. Herman, S.A. Kinne, and D.J. Hofmann, Pinatubo and pre-Pinatubo optical depth spectra: Mauna Loa measurements, comparisons, inferred particle size distributions, radiative effects, and relationship to lidar data, *J. Geophys. Res.*, *98*, 22969-22985, 1993a.

Russell, P.B., J.M. Livingston, R.F. Pueschel, J.A. Reagan, E.V. Browell, G.C. Toon, P.A. Newman, M.R. Schoeberl, L.R. Lait, L. Pfister, Q. Gao, and B.M. Herman, Post-Pinatubo optical depth spectra vs. latitude and vortex structure: Airborne tracking sunphotometer measurements in AASE II, *Geophys. Res. Lett.*, *20*, 2571-2574, 1993b.

Russell, P.B., J.M. Livingston, R.F. Pueschel, J.B. Pollack, S. Brooks, P. Hamill, J. Hughes, L. Thomason, L. Stowe, T. Deshler, and E. Dutton, Global to microscale evolution of the Pinatubo volcanic aerosol, derived from diverse measurements and analyses, *J. Geophys. Res.*, *101*, 18745-18763, 1996.

Santee, M.L., A. Tabazadeh, G.L. Manney, R.J. Salawitch, L. Froidevaux, W.G. Read, and J.W. Waters, UARS Microwave Limb Sounder HNO_3 observations: Implications for Antarctic PSCs, *J. Geophys. Res.*, *103*, 13285-13313, 1998.

Sassen, K., D.O'C. Starr, G.G. Mace, M.R. Poellot, S.H. Melfi, W.L. Eberhard, J.D. Spinhirne, E.W. Eloranta, D.E. Hagen, and J. Hallett, The 5-6 December 1991 FIRE IFO II jet stream cirrus case study: Possible influences of volcanic aerosols, *J. Atmos. Sci.*, *52*, 97-123, 1995.

Schlager, H., F. Arnold, D.J. Hofmann, and T. Deshler, Balloon observations of nitric acid aerosol formation in the Arctic stratosphere: I, Gaseous nitric acid, *Geophys. Res. Lett.*, *17*, 1275-1278, 1990.

Sheridan, P.J., R.C. Schnell, D.J. Hofmann, and T. Deshler, Electron microscope studies of Mt. Pinatubo aerosol layers over Laramie, Wyoming during summer 1991, *Geophys. Res. Lett.*, *19*, 203-206, 1992.

Sheridan, P.J., C.A. Brock, and J.C. Wilson, Aerosol particles in the upper troposphere and lower stratosphere: Elemental composition and morphology of individual particles in northern midlatitudes, *Geophys. Res. Lett.*, *21*, 2587-2590, 1994.

Shibata, T., Y. Iwasaka, M. Fujiwara, M. Hayashi, M. Nagatani, K. Shiraishi, J. Adachi, T. Sakai, K. Susumu, and Y. Nakura, Polar stratospheric clouds observed by lidar over Spitsbergen in the winter 1994/95: Liquid particles and vertical "sandwich" structure, *J. Geophys. Res.*, *102*, 10829-10840, 1997.

Solomon, S., S. Borrmann, R.R. Garcia, R. Portmann, L. Thomason, L.R. Poole, D. Winker, and M.P. McCormick, Heterogeneous chlorine chemistry in the tropopause region, *J. Geophys. Res.*, *102*, 21411-21429, 1997.

Stanford, J.L., and J.S. Davis, A century of stratospheric cloud reports: 1870-1972, *Bull. Amer. Meteorol. Soc.*, *55*, 213-219, 1974.

Stebel, K., O. Schrems, R. Neuber, G. Beyrle, J. Biele, I. Beninga, H. Schütt, and P. von der Gathen, Polar stratospheric clouds above Spitsbergen, in *Atmospheric Ozone: Proceedings of the XVIII Quadrennial Ozone Symposium*, edited by R.D. Bojkov and G. Visconti, pp. 607-610, Parco Scientifico e Technologico d'Abruzzo, L'Aquila, Italy, 1998.

Steele, H.M., and P. Hamill, Effects of temperature and humidity on the growth and optical properties of sulfuric acid-water droplets in the stratosphere, *J. Aerosol Sci.*, *12*, 517-528, 1981.

Stefanutti, L., M. Morandi, M. Del Guasta, S. Godin, G. Mégie, J. Brechet, and J. Piquard, Polar stratospheric cloud observations over the Antarctic continent at Dumont d'Urville, *J. Geophys. Res.*, *96*, 12975-12987, 1991.

Stefanutti, L., M. Morandi, M. Del Guasta, S. Godin, and C. David, Unusual PSCs observed by lidar in Antarctica, *Geophys. Res. Lett.*, *22*, 2377-2380, 1995.

Stein, B., M. Del Guasta, J. Kolenda, M. Morandi, P. Rairous, L. Stefanutti, J.P. Wolf, and L. Wöste, Stratospheric aerosol size distributions from multispectral lidar measurements at Sodankylä during EASOE, *Geophys. Res. Lett.*, *21*, 1311-1314, 1994.

Stein, B., F. Immler, B. Mielke, P. Rairoux, C. Wedekind, L. Wöste, M. del Guasta, M. Morandi, L. Stefanutti, F. Masci, V. Rizi, R. Matthey, V. Mitev, M. Douard, J.P. Wolf, and E. Kyrö, Microlayers of solid particles observed by lidar at Sodankylä during SESAME, in *Polar Stratospheric Ozone 1995*, Air Pollution Research Report 56, edited by J.A. Pyle, N.R.P. Harris, and G.T. Amanatidis, pp. 132-135, European Commission, 1995.

Stothers, R.B., Major optical depth perturbations to the stratosphere from volcanic eruptions: Pyrheliometric period, 1881-1960, *J. Geophys. Res.*, *101*, 3901-3920, 1996.

Stowe, L.L., R.M. Carey, and P.P. Pellegrino, Monitoring the Mt. Pinatubo aerosol layer with NOAA/11 AVHRR data, *Geophys. Res. Lett.*, *19*, 159-162, 1992.

Tabazadeh, A., and O.B. Toon, The presence of HNO_3/H_2O solid phases in the stratosphere inferred from ER-2 data, *J. Geophys. Res.*, *101*, 9071-9078, 1996.

Tabazadeh, A., R.P. Turco, and M.Z. Jacobson, A model for studying the composition and chemical effects of stratospheric aerosols, *J. Geophys. Res.*, *99*, 12897-12914, 1994.

Tabazadeh, A., O.B. Toon, and P. Hamill, Freezing behavior of stratospheric sulfate aerosols inferred from trajectory studies, *Geophys. Res. Lett.*, *22*, 1725-1725, 1995.

Tabazadeh, A., O.B. Toon, B.L. Gary, J.T. Bacmeister, and M.R. Schoeberl, Observational constraints on the formation of Type 1a polar stratospheric clouds, *Geophys. Res. Lett.*, *23*, 2109-2112, 1996.

Taylor, F.W., A. Lambert, R.G. Grainger, C.D. Rodgers, and J.J. Remedios, Properties of Northern Hemisphere stratospheric clouds and volcanic aerosol in 1991/92 from UARS/ISAMS satellite measurements, *J. Atmos. Sci.*, *51*, 3019-3026, 1994.

Thomason, L.W., and L.R. Poole, Use of stratospheric aerosol properties as diagnostics of Antarctic vortex processes, J. *Geophys. Res.*, *98*, 23003-23012, 1993.

Thomason, L.W., L.R. Poole, and T. Deshler, A global climatology of stratospheric aerosol surface area density deduced from Stratospheric Aerosol and Gas Experiment II measurements: 1984-1994, *J. Geophys. Res.*, *102*, 8967-8976, 1997a.

Thomason, L.W., G.S. Kent, C.R. Trepte, and L.R. Poole, A comparison of the stratospheric aerosol background periods of 1979 and 1989-1991, *J. Geophys. Res.*, *102*, 3611-3616, 1997b.

Tie, X.X., G.P. Brasseur, B. Briegleb, and C. Granier, 2-dimensional simulation of Pinatubo aerosol and its effect on stratospheric ozone, *J. Geophys. Res.*, *99*, 20545-20562, 1994.

Toon, O.B., and M.A. Tolbert, Spectroscopic evidence against nitric acid trihydrate in polar stratospheric clouds, *Nature*, *375*, 218-221, 1995.

Toon, O.B., E.V. Browell, S. Kinne, and J. Jordan, An analysis of lidar observations of polar stratospheric clouds, *Geophys. Res. Lett.*, *17*, 393-396, 1990.

Toon, O., E. Browell, B. Gary, L. Lait, J. Livingston, P. Newman, R. Pueschel, P. Russell, M. Schoeberl, G. Toon, W. Traub, F.P.J. Valero, H. Selkirk, and J. Jordan, Heterogeneous reaction probabilities, solubilities, and the physical state of cold volcanic aerosols, *Science*, *261*, 1136-1140, 1993.

Trepte, C.R., and M.H. Hitchman, Tropical stratospheric circulation deduced from satellite aerosol data, *Nature*, *355*, 626-628, 1992.

Trepte, C.R., R.E. Veiga, and M.P. McCormick, The poleward dispersal of Mount Pinatubo volcanic aerosol, *J. Geophys. Res.*, *98*, 18563-18573, 1993.

Turco, R.P., P. Hamill, O.B. Toon, R.C. Whitten, and C.S. Kiang, A one-dimensional model describing aerosol formation and evolution in the stratosphere: I, Physical processes and mathematical analogs, *J. Atmos. Sci.*, *36*, 699-717, 1979.

Turco, R.P., R.C. Whitten, and O.B. Toon, Stratospheric aerosols: Observations and theory, *Rev. Geophys. Space Phys.*, *20*, 233-279, 1982.

Turco, R.P., O.B. Toon, and P. Hamill, Heterogeneous physicochemisty of the polar ozone hole, *J. Geophys. Res.*, *94*, 16493-16510, 1989.

Twomey, S.A., Information content in remote sensing, *Appl. Opt.*, *13*, 942-945, 1974.

Twomey, S.A., *Introduction to the Mathematics of Inversion in Remote Sensing and Indirect Measurements*, 243 pp., Elsevier Science, New York, 1977.

Uchino, O., T. Nagai, T. Fujimoto, W.A. Matthews, and J. Orange, Extensive lidar observations of the Pinatubo aerosol layers at Tsukuba (36.1˚N), Naha (26.2˚N), Japan, and Lauder (45.0˚S), New Zealand, *Geophys. Res. Lett.*, *22*, 57-60, 1995.

Vaughan, G., D.P. Wareing, S.B. Jones, L. Thomas, and N. Larsen, Lidar measurements of Mt. Pinatubo aerosols at Aberystwyth from August 1991 through March 1992, *Geophys. Res. Lett.*, *21*, 1315-1318, 1994.

Vitt, F.M., and C.H. Jackman, A comparison of sources of odd-nitrogen production from 1974 through 1993 in the Earth's middle atmosphere as calculated using a 2-dimensional model, *J. Geophys. Res.*, *101*, 6729-6739, 1996.

Volkert, H., and D. Intes, Orographically forced stratospheric waves over northern Scandinavia, *Geophys. Res. Lett.*, *19*, 1205-1208, 1992.

Volz, F.E., and R.M. Goody, The intensity of the twilight and upper atmospheric dust, *J. Atmos. Sci.*, *19*, 385-406, 1962.

Wandinger, U., A. Ansmann, J. Reichadt, and T. Deshler, Determination of stratospheric aerosol microphysical properties from independent extinction and backscattering measurements with a Raman lidar, *Appl. Opt.*, *34*, 8315, 1995.

Wang, P.H., P. Minnis, M.P. McCormick, and G.S. Kent, A 6-year climatology of cloud occurrence frequency from Stratospheric Aerosol and Gas Experiment II observations (1985-1991), *J. Geophys. Res.*, *101*, 29407-29429, 1996.

Wedekind, C., F. Immler, B. Mielke, P. Rairoux, B. Stein, L. Wöste, M. Del Guasta, M. Morandi, L. Stefanutti, F. Masci, V. Rizi, R. Matthey, V. Mitev, M. Douard, J.P. Wolf, and E. Kyrö, Polar stratospheric cloud measurements by multispectral lidar in Sodankylä in winter 1994/95, in *Advances in Atmospheric Remote Sensing with Lidar*, edited by A. Ansmann, R. Neuber, P. Rairoux, and U. Wandinger, pp. 513-516, Springer-Verlag, Berlin, 1997.

Weisenstein, D.K., G.K. Yue, M.K.W. Ko, N.-D. Sze, J.M. Rodriguez, and C.J. Scott, A two-dimensional model of sulfur species and aerosols, *J. Geophys. Res.*, *102*, 13019-13035, 1997.

Wennberg, P.O., R.C. Cohen, R.M. Stimpfle, J.P. Koplow, J.G. Anderson, R.J. Salawitch, D.W. Fahey, E.L. Woodbridge, E.R. Keim, R.S. Gao, C.R. Webster, R.D. May, D.W. Toohey, L.M. Avallone, M.H. Proffitt, M. Loewenstein, J.R. Podolske, K.R. Chan, and S.C. Wofsy, Removal of stratospheric O_3 by radicals: In situ measurements of OH, HO_2, NO, NO_2, ClO, and BrO, *Science*, *266*, 398-404, 1994.

Wilson, J.C., J.H. Hyun, and E.D. Blackshear, The function and response of an improved stratospheric condensation nuclei counter, *J. Geophys. Res.*, *88*, 6781-6785, 1983.

Wilson, J.C., M. Loewenstein, D.W. Fahey, B. Gary, S.D. Smith, K.K. Kelly, G.V. Ferry, and K.R. Chan, Observations of condensation nuclei in the Airborne Antarctic Ozone Experiment: Implications for new particle formation and polar stratospheric cloud formation, *J. Geophys. Res.*, *94*, 16437-16448, 1989.

Wilson, J.C., M.R. Stoltzenburg, W.E. Clark, M. Loewenstein, G.V. Ferry, K.R. Chan, and K.K. Kelly, Stratospheric sulfate aerosol in and near the Northern Hemisphere polar vortex: The morphology of the sulfate layer, multimodal size distributions, and the effect of denitrification, *J. Geophys. Res.*, *97*, 7997-8013, 1992.

Wilson, J.C., H.H. Jonsson, C.A. Brock, D.W. Toohey, L.M. Avallone, D. Baumgardner, J.E. Dye, L.R. Poole, D.C. Woods, R.J. DeCoursey, M. Osborn, M.C. Pitts, K.K. Kelly, K.R. Chan, G.V. Ferry, M. Loewenstein, J.R. Podolske, and A. Weaver, In situ observations of aerosol and chlorine monoxide after the 1991 eruption of Mount Pinatubo: Effect of reactions on sulfate aerosol, *Science*, *261*, 1140-1143, 1993.

WMO (World Meteorological Organization), *Scientific Assessment of Ozone Depletion: 1994*, Global Ozone Research and Monitoring Project—Report No. 37, Geneva, 1995.

Wofsy S.C., R.J. Salawitch, J.H. Yatteau, M.B. McElroy, B.W. Gandrud, J.E. Dye, and D. Baumgardner, Condensation of HNO_3 on falling ice particles: Mechanisms for denitrification of the polar stratosphere, *Geophys. Res. Lett.*, *17*, 449-460, 1990.

Young, A.T., Revised depolarization corrections for atmospheric extinction, *Appl. Opt.*, *19*, 3427-3428, 1980.

Young, R.E., H. Houben, and O.B. Toon, Radiatively forced dispersion of the Mt. Pinatubo volcanic cloud and induced temperature perturbations in the stratosphere during the first few months following the eruption, *Geophys. Res. Lett.*, *21*, 369-372, 1994.

Yue, G.K., L.W. Thomason, L.R. Poole, P.H. Wang, D. Baumgardner, and J.E. Dye, Aerosol surface areas deduced from early 1993 SAGE II data and comparisons with stratospheric photochemistry, aerosols, and Dynamics Expedition measurements, *Geophys. Res. Lett.*, *22*, 2933-2936, 1995.

Zander, R., C.P. Rinsland, C.B. Farmer, J. Namkung, R.H. Norton, and J.M. Russell III, Concentrations of carbonyl sulfide and hydrogen cyanide in the free upper troposphere and lower stratosphere deduced from ATMOS/Spacelab 3 infrared solar occultation spectra, *J. Geophys. Res.*, *93*, 1669-1678, 1988.

Zhang, R., P.J. Wooldridge, J.P.D. Abbatt, and M.J. Molina, Physical chemistry of the H_2SO_4/H_2O binary system at low temperatures: Stratospheric implications, *J. Phys. Chem.*, *97*, 7351-7358, 1993.

Zhang, R.Y., M.T. Leu, and M.J. Molina, Formation of polar stratospheric clouds on preactivated background aerosols, *Geophys. Res. Lett.*, *23*, 1669-1672, 1996.

Zhao, J., O.B. Toon, and R.P. Turco, Origin of condensation nuclei in the springtime polar stratosphere, *J. Geophys. Res.*, *100*, 5215-5227, 1995.

Zolensky, M.E., D.S. McKay, and L.A. Kaczor, A tenfold increase in the abundance of large solid particles in the stratosphere, as measured over the period 1976-1984, *J. Geophys. Res.*, *94*, 1047-1056, 1989.